A Discrete Model for the Efficient Analysis of Time-Varying Narrowband Communication Channels*

Niklas Grip and Götz E. Pfander

22nd December 2005

Abstract

We derive an efficient numerical algorithm for the analysis of certain classes of Hilbert–Schmidt operators that naturally occur in models of wireless radio and sonar communications channels.

A common short-time model of these channels writes the channel output as a weighted superposition of time- and frequency shifted copies of the transmitted signal, where the weight function is usually called the *spreading function* of the channel operator.

It is often believed that a good channel model must allow for spreading functions containing Dirac delta distributions. However, we show that many narrowband finite lifelength systems such as wireless radio communications can be well modelled by smooth and compactly supported spreading functions.

Further, we exploit this fact to derive a fast algorithm for computing the matrix representation of such operators with respect to well time-frequency localized Gabor bases (such as pulseshaped OFDM bases). Hereby we use a minimum of approximations, simplifications, and assumptions on the channel. Finally, we provide and discuss some sample plots from a MATLAB implementation which is fast enough for channels and communication systems of sizes typically in use today.

The derived algorithm and software can be used, for example, for comparing how different system settings and pulse shapes affect the diagonalization properties of an OFDM system acting on a given channel.

Keywords: communication channel discretization, Gabor systems, Hilbert–Schmidt operators, diagonalization, spreading function, BEM (Basis Expansion Model), OFDM, DMT, channel model, mobile phone communications, satellite communications, underwater sonar communications.

*The work on this project was supported by the German Research Foundation (DFG) Project PF 450/1-1 as part of the DFG priority program TakeOFDM.

Contents

1 Introduction

Channel–dependent customization is expected to provide considerable performance improvements in time-varying systems such as future generations of wireless communications systems. Consequently, the idea of shaping the transmission pulses in order to minimize the InterCarrier and InterSymbol Interference (ISI and ICI) in Orthogonal Frequency Division Multiplexing (OFDM) communications is an active research area in the applied harmonic analysis and signal processing communities (see [BS01, MSG+05] and references therein). Even though some insights can be gained from careful mathematical modelling and analysis, there remains a need for fast algorithms and implementations aimed at the numerical evaluation of performance improvements through pulseshaping. In this paper, we discuss two closely connected topics that we regard of vital importance to fulfill this demand.

1. We review the most important physical properties of wireless channels and show how these lead naturally to a model of the short-time behavior of a channel as an operator H that maps an input signal s to a weighted superposition of time and frequency shifts of s, that is,

$$Hs(\cdot) = \int_{K\times[A,\infty)} S_H(\nu,t)\, \mathrm{e}^{i2\pi\nu(t-t_0)} s(\,\cdot\, - t)\, \mathrm{d}(\nu,t)\,, \qquad K \text{ compact.} \quad (1.1)$$

This model is well-known and the coefficient function S_H is usually called the *spreading function* of H. The model given by (1.1) is mostly used either under the assumption that S_H is square-integrable or that S_H is a tempered distribution. The latter, weaker assumption suggests that the input signal s should be a Schwartz class function and requires the use of distribution theory in the analysis of H, both of which we shall try to avoid. Therefore, we derive (1.1) using some refinements of the standard multipath propagation model of the channel. Our analysis implies that the short-time behaviour in many communications applications can be completely described by a smooth S_H with rapid decay ensuring "essentially compact" support[1]. This model has the big advantage that it allows for *both* Fourier analysis and numerical evaluation of the performance of OFDM procedures without the need of deviating into distribution theory.

2. We employ the channel model described above to derive an efficient algorithm for the numerical evaluation of ISI and ICI in pulseshaped OFDM systems.

We shall now motivate and describe the principles of our discretization in some detail:

For multicarrier modulation systems in general, the aim is the joint diagonalization of a class of possible channel operators in a given environment. That is, we try to find a transmission basis (g_i) and a receiver basis (filters) $(\widetilde{\gamma}_j)$ with the property that all coefficient mappings that correspond to channels in the environment have

[1] With *essentially compact* we mean that the function decays fast enough to assure that in any practical application, the function values outside some "reasonably small" compact set are very small compared to the overall noise level and therefore negligible (see also Section 6.1).

matrix representations $\mathrm{G}_{i,j} = \langle Hg_i, \widetilde{\gamma}_j \rangle$ that are as close to diagonal as possible, that is, $|\mathrm{G}_{i,j}|$ decays fast with $|i-j|$. In general, an easily computable inverse of this coefficient mapping would allow us to regain the transmitted coefficients (c_i) in the input signal $s = \sum c_i g_i$, and, therefore, the information embedded in these coefficients, from the inner products $\langle Hs, \widetilde{\gamma}_i \rangle$ which are calculated on the receiver side.

In wireline communications, the problem described above has a well accepted solution, namely OFDM (also called Discrete MultiTone or DMT) with cyclic prefix. Here, the transmission basis (g_i) and the receiver basis (γ_i) are so-called Gabor bases, that is, each basis consists of time and frequency shifts of a single prototype function which is often referred to as window function. Diagonalization of the channel operator using Gabor bases with rectangular prototype function is then possible since wired channels are assumed to be time-invariant. This allows us to model such channel operators as convolution operators with complex exponentials $\mathrm{e}^{\mathrm{i}2\pi\omega t}$ as "eigenfunctions". This cyclic prefix procedure applies if the channel has finite lifelength and is explained in more detail in Section 4.1 and with further references in [Gri02]. The superiority of Gabor bases in comparison to Wavelet and Wilson bases for wireline communications is examined in detail in [KPZ02].

Wireless channels are inherently time-varying. The generality of time-varying channel operators and, in particular, the fact that they do not commute in general, implies that joint diagonalization of classes of such channels cannot be achieved as in the general case, so approximate diagonalization becomes our goal. In many cases, for example in mobile telephony, the channel varies only "slowly" with time. Hence, we use the results for time-invariant channels as a starting point and consider in this paper only the use of Gabor bases as transmitter and receiver bases.

For such slowly time-varying systems, Matz, Schafhuber, Gröchenig, Hartmann and Hlawatsch conclude that excellent joint time-frequency concentration of the windows g and γ is the most important requirement for low ISI and ICI [MSG+05]. There, it is shown how to compute a γ (or an orthogonalization of the basis (g_i)) that diagonalizes the coefficient mapping in the idealized borderline case when the channel is the identity operator ($[H]_{i,j} = \delta_{i,j}$). They show that both γ and the corresponding orthogonalized basis inherit certain polynomial or subexponential time-frequency decay properties from g. They also derive exact and approximate expressions for the ISI and ICI and present an efficient FFT-based modulator and demodulator implementation.

For multicarrier systems with excellent joint time-frequency localization of g and γ, we derive, starting from our channel model, a procedure for the *numerical* computation of the matrix entries $\mathrm{G}_{i,j} = \langle Hg_i, \widetilde{\gamma}_j \rangle$ under a minimum of assumptions, simplifications, or approximations. We derive our algorithm in a multivariate setting for potential use in other theoretical or practical applications that use a time-variant impulse response model (such as the condition monitoring applications in cf. [CBWB99, CBB01, CB00, CBUB+02, MH99]). These properties make our approach different from and complementary to a number of papers that use *discrete* Gabor bases (sometimes under the name BEM or Basis Expansion Model) for time-varying channels and statistical applications, such as [BLM04, BLM05, LM04, LZG03, MG02, MG03b, MG03a, MLG05, SA99, TL04].

The paper is organized as follows: The Notation and some mathematical preliminaries are described in *Section 2*. We derive a channel model in *Section 3*, and use it to derive formulas for the matrix elements in *Section 4*. In *Section 5* we describe a MATLAB implementation of these formulas and give suggestions on how to do the necessary parameter and window/pulseshape choices. In *Section 6* we provide typical system-dependent parameters for and demonstrate our software on some example mobile phone communications, satellite communications and underwater sonar communications applications. Finally, our conclusions follow in *Section 7*.

2 Preliminaries

For completeness and easy availability we collect our notation in Section 2.1 and give an overview of the mathematical tools that we shall use. In Section 2.2 we shall discuss the availability of functions that are compactly supported and "essentially bandlimited", in particular, we explain how compactly supported functions can be designed to have subexponential decay. Section 2.3 covers the Gabor system expansions which are used to obtain diagonal dominant coefficient mappings of channel operators. Finally, in Section 2.4 we discuss the Hilbert–Schmidt operator theory and the integral representation of channel operators in terms of system functions such as the spreading function and the time-varying impulse response.

2.1 Notation

We assume the reader to know some basic tools and notation from functional analysis and measure theory, which otherwise can be found in [Fol99, Rud87].

The conjugate of a complex number z is denoted $\overline{z}$. We use boldface font for elements in $\mathbb{R}^d$, write $\mathbb{R}_+^d \stackrel{\text{def}}{=} (0,\infty)^d \stackrel{\text{def}}{=} \mathbb{R}_+ \times \mathbb{R}_+ \times \cdots \times \mathbb{R}_+$ and $\mathbb{Z}_+^d \stackrel{\text{def}}{=} \mathbb{Z}^d \cap \mathbb{R}_+^d$. The Fourier transform of a function f is formally given by $\widehat{f}(\boldsymbol{\xi}) = \int_{\mathbb{R}^d} f(\boldsymbol{t}) \mathrm{e}^{-i2\pi\langle \boldsymbol{\xi},\boldsymbol{t}\rangle}\, \mathrm{d}\boldsymbol{t}$ for $\boldsymbol{\xi} \in \mathbb{R}^d$ and $l^2 \stackrel{\text{def}}{=} l^2(\mathbb{Z}^d \times \mathbb{Z}^d)$ is the Hilbert space of sequences $(c_{\boldsymbol{q},\boldsymbol{r}})$ for which the l^2-norm is given by

$$\|(c_{\boldsymbol{q},\boldsymbol{r}})\|_2 \stackrel{\text{def}}{=} \left(\sum_{\boldsymbol{q},\boldsymbol{r} \in \mathbb{Z}^d} |c_{\boldsymbol{q},\boldsymbol{r}}|^2 \right)^{1/2} < \infty.$$

Throughout the paper we use Roman and Greek letters for variables that have a physical interpretation as time or spacial variable and frequency, respectively. For

$\boldsymbol{A}, \boldsymbol{B}, \boldsymbol{C}, \boldsymbol{x}, \boldsymbol{y}, \boldsymbol{t}, \boldsymbol{\nu}, \boldsymbol{\omega} \in \mathbb{R}^d$ and $r \in \mathbb{R}$ we use the following shorthand notation:

$$
\begin{aligned}
[\boldsymbol{A}, \boldsymbol{B}] &\stackrel{\text{def}}{=} [A_1, B_1] \times \cdots \times [A_d, B_d], & \mathbf{1} &\stackrel{\text{def}}{=} \begin{pmatrix} 1 & 1 & \cdots & 1 \end{pmatrix}^T, \\
\langle \boldsymbol{x}, \boldsymbol{y} \rangle &\stackrel{\text{def}}{=} x_1 y_1 + x_2 y_2 + \cdots + x_d y_d, & \boldsymbol{x}\boldsymbol{y} &\stackrel{\text{def}}{=} \begin{pmatrix} x_1 y_1 & \cdots & x_d y_d \end{pmatrix}^T \\
\frac{\boldsymbol{x}}{r} &\stackrel{\text{def}}{=} \begin{pmatrix} \frac{x_1}{r} & \frac{x_2}{r} & \cdots & \frac{x_d}{r} \end{pmatrix}^T, & \boldsymbol{x}^r &\stackrel{\text{def}}{=} \begin{pmatrix} x_1^r & x_2^r & \cdots & x_d^r \end{pmatrix}^T, \\
\frac{\boldsymbol{x}}{\boldsymbol{y}} &\stackrel{\text{def}}{=} \begin{pmatrix} \frac{x_1}{y_1} & \frac{x_2}{y_2} & \cdots & \frac{x_d}{y_d} \end{pmatrix}^T, & |\boldsymbol{x}| &\stackrel{\text{def}}{=} x_1 x_2 \cdots x_d, \\
T_{\boldsymbol{t}} g &\stackrel{\text{def}}{=} g(\cdot - \boldsymbol{t}), & M_{\boldsymbol{\nu}} g &\stackrel{\text{def}}{=} g(\cdot) \mathrm{e}^{\mathrm{i}2\pi\langle \boldsymbol{\nu}, \cdot \rangle}, \\
I_{\boldsymbol{C},\boldsymbol{B}} &\stackrel{\text{def}}{=} \left[\boldsymbol{C} - \frac{\boldsymbol{B}}{\mathbf{2}}, \boldsymbol{C} + \frac{\boldsymbol{B}}{\mathbf{2}} \right] \quad \text{and} & \operatorname{sinc}_{\boldsymbol{\omega}}(\boldsymbol{x}) &\stackrel{\text{def}}{=} \prod_{j=1}^{d} \frac{\sin(\pi \omega_j x_j)}{\pi x_j}.
\end{aligned}
$$

Here, $\operatorname{sinc}_{\boldsymbol{\omega}}$ is extended continuously to $\mathbb{R}^d$ and we shall frequently use that

$$
\int_{I_{\boldsymbol{C},\boldsymbol{B}}} \mathrm{e}^{-\mathrm{i}2\pi\langle \boldsymbol{\xi}, \boldsymbol{x} \rangle} \, \mathrm{d}\boldsymbol{\xi} = \mathrm{e}^{-\mathrm{i}2\pi\langle \boldsymbol{C}, \boldsymbol{x} \rangle} \operatorname{sinc}_{\boldsymbol{B}}(\boldsymbol{x}). \tag{2.1}
$$

For $\epsilon > 0$ we define the *ϵ-essential support* of a bounded function $f \colon \mathbb{R}^d \to \mathbb{C}$ to be the closure of the set $\{ \boldsymbol{x} : \epsilon \le |f(\boldsymbol{x})| \,/\, \sup_{\boldsymbol{x}} |f(\boldsymbol{x})| \}$. For an almost everywhere defined function f, $\operatorname{supp} f$ denotes the intersection of the supports of all representatives of f (and similarly for ϵ-essential support). For any set I, χ_I is the characteristic function $\chi_I(\boldsymbol{x}) = 1$ if $\boldsymbol{x} \in I$ and $\chi_I(\boldsymbol{x}) = 0$ otherwise. The sets of n times, respectively infinitely many, times continuously differentiable functions are denoted C^n and C^∞, respectively.

We denote by $L^p = L^p(\mathbb{R}^d)$ the Banach space of complex-valued measurable functions f with norm

$$
\|f\|_p \stackrel{\text{def}}{=} \left(\int_{\mathbb{R}^d} |f(\boldsymbol{x})|^p \, \mathrm{d}\boldsymbol{x} \right)^{1/p} < \infty.
$$

$L^2(\mathbb{R}^d)$ is a Hilbert space with inner product $\langle f, g \rangle \stackrel{\text{def}}{=} \int_{\mathbb{R}^d} f(\boldsymbol{x}) \overline{g(\boldsymbol{x})} \, \mathrm{d}\boldsymbol{x}$. We say that two sequences $(f_{\boldsymbol{n}})$ and $(g_{\boldsymbol{n}})$ of functions are *biorthogonal* if $\langle f_{\boldsymbol{m}}, g_{\boldsymbol{n}} \rangle = 0$ whenever $\boldsymbol{m} \neq \boldsymbol{n}$ and $\langle f_{\boldsymbol{n}}, g_{\boldsymbol{n}} \rangle = 1$ for all $\boldsymbol{n}$. The Wiener amalgam space $W(A, l^1) = S_0(\mathbb{R}^d)$ (also named the Feichtinger algebra) consists of the set of all continuous $f \colon \mathbb{R}^d \to \mathbb{C}$ for which

$$
\sum_{\boldsymbol{n} \in \mathbb{Z}^d} \| (f(\cdot) \psi(\cdot - \boldsymbol{n}))\hat{} \|_1 < \infty
$$

for some compactly supported ψ such that $\widehat{\psi} \in L^1(\mathbb{R}^d)$ and $\sum_{n \in \mathbb{Z}^d} \psi(\boldsymbol{x} - \boldsymbol{n}) = 1$. We write S_0' for the space of linear bounded functionals on S_0. S_0 is also a so-called modulation space, described at more depth and with notation $S_0 = M^{1,1} = M^1$ and $S_0' = M^{\infty,\infty} = M^\infty$ in [Grö00, FZ98].

A real-valued, measurable and locally bounded function w on $\mathbb{R}^d$ is said to be a *weight function* if for all $\boldsymbol{x}, \boldsymbol{y} \in \mathbb{R}^d$,

$$
w(\boldsymbol{x}) \ge 1 \qquad \text{and} \qquad w(\boldsymbol{x} + \boldsymbol{y}) \le w(\boldsymbol{x}) w(\boldsymbol{y}). \tag{2.2}
$$

For weight functions w we define $L^1_w = L^1_w(\mathbb{R}^d)$ to be the family of functions $f \in L^1(\mathbb{R}^d)$ such that

$$\|f\|_{1,w} \stackrel{\text{def}}{=} \|fw\|_1 < \infty.$$

2.2 Frequency localization of compactly supported functions

The Gabor window g in the introduction needs to be compactly supported in a time interval short enough to satisfy typical maximum delay restrictions, such as 25 ms for voice communications. Moreover, its Fourier transform $\widehat{g}$ has to decay fast enough to allow for reasonably high transmission power (which determines the signal-to-noise ratio) without exceeding standard regulations on the allowed power leakage into other frequency bands. In other words, g should have good, joint time-frequency localization, which also is of great importance for achieving low ISI and ICI [MSG+05]. For this reason, we seek to know to what extent compact support of a function can be combined with good decay of its Fourier transform. This classical question was first answered by Beurling [Beu38, Theorem V B] and generalized from functions on $\mathbb{R}$ to functions on locally compact abelian groups, such as $\mathbb{R}^d$, by Domar [Dom56, Theorem 2.11]. Domar's results are explained in much more detail in [RS00, Ch. 6.3 + appendices]. One way to measure the speed of decay of a Fourier transform is to check for how fast growing weight functions w it belongs to $L^1_w(\mathbb{R})$. To describe a function's asymptotic decay, we only need to consider continuous w such that $w(\xi)$ and $w(-\xi)$ are nondecreasing for positive ξ. The following theorem can be obtained from a combination of a similar result [RS00, Theorem A.1.13] for locally compact abelian groups with the here added continuity and decay assumptions on w (see [GP05] for a proof).

Theorem 1. *Let w be a continuous weight function such that $w(\xi)$ and $w(-\xi)$ are nondecreasing for positive ξ. Suppose that there is a non-zero compactly supported function $f \in L^2(\mathbb{R})$ such that $\widehat{f} \in L^1_w(\mathbb{R})$. Then*

$$\int_{\mathbb{R}} \frac{\log(w(\xi))}{1+\xi^2}\, d\xi < \infty. \tag{2.3}$$

The so-called *logarithmic integral condition* (2.3) limits the decay of *both* the amplitude and "the area under the tail" of $\widehat{f}$. For example, the Fourier transform of a compactly supported function f cannot be either $\mathcal{O}(\mathrm{e}^{-\alpha|\xi|})$ nor $\widehat{f}(\xi) = \sum_{n\in\mathbb{Z}} \phi(\mathrm{e}^{\alpha|n|}(\xi - n))$ for any $\phi \in C^\infty$ with support $\operatorname{supp}\phi \in [0,1]$, because in both cases, $\widehat{f} \in L^1_w(\mathbb{R})$ for $w(\xi) = \mathrm{e}^{a|\xi|}$ and $a < \alpha$ but w does not satisfy (2.3). This fact rules out the existence of compactly supported functions f with exponentially decaying $\widehat{f}$. However, Dziubański and Hernández [DH98] have shown how to use a construction by Hörmander [Hör03, Theorem 1.3.5] to construct a compactly supported function f whose Fourier transform is *subexponentially decaying*. That is, they construct f such that for every $0 < \varepsilon < 1$ there exists $C_\varepsilon > 0$ such that

$$\left|\widehat{f}(\xi)\right| \le C_\varepsilon \mathrm{e}^{-|\xi|^{1-\varepsilon}}, \qquad \forall \xi \in \mathbb{R}.$$

From their example and standard techniques such as convolution with a characteristic function, it is then easy to design for any compact set K a compactly supported function f such that $f(x) = 1$ for $x \in K$, and $\widehat{f}$ is subexponentially decaying.

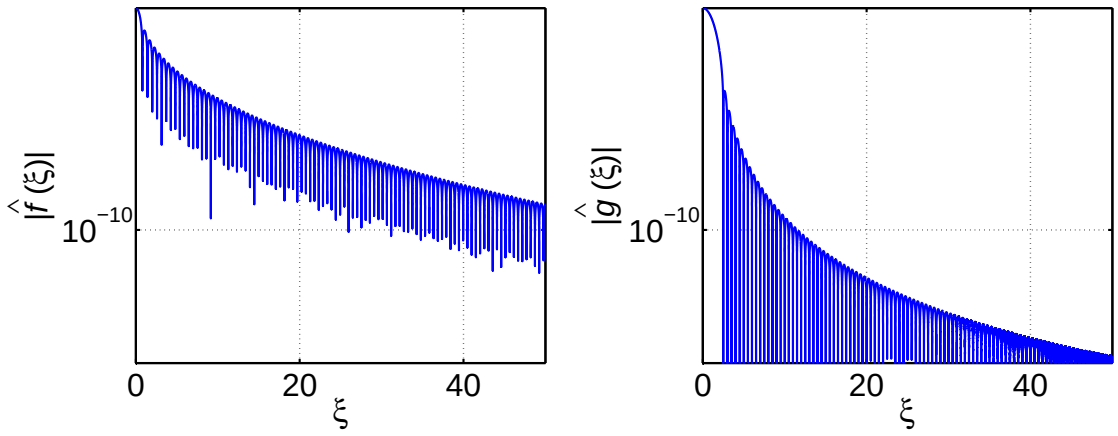

(a) (b)

Figure 1: The Fourier transform decay after normalizing the following positive functions to have integral 1: (a) $f(x) \stackrel{\text{def}}{=} e^{-\frac{1}{1-x^2}}\chi_{[-1,1]}(x)$. (b) $g(x) = (1+\cos(\pi x))^4\chi_{[-1,1]}(x)$.

Note however, that subexponential decay is not everything. For example, the function $f(x) = \mathrm{e}^{-\frac{1}{1-x^2}}\chi_{[-1,1]}(x)$ is a compactly supported C^∞ function, so that $\widehat{f}(\xi) = \mathcal{O}(1+|\xi|)^{-n}$ for all $n \in \mathbb{N}$, whereas the function $g(x) = (1+\cos(\pi x))^4\chi_{[-1,1]}(x)$ is only four times continuously differentiable, so $\widehat{g} = \mathcal{O}(1+|x|)^{-n}$ only for $0 \le n \le 4$. However, Figure 1 shows that $\widehat{g}$ decays much faster down to amplitude thresholds such as the power leakage restrictions described above (see also Figure 7, page 33). Thus it can be an important design issue to choose functions and forms of decay that are optimal for a given application.

However, for simplicity and a clear presentation in this paper, we shall consistently claim subexponential decay although also other forms of decay are rapid enough for all of our results to hold.

2.3 Gabor analysis

Here, we give a brief review of some basic Gabor frame theory that is needed to understand the relevance of the coefficient mappings that we introduce in (2.6) below. For a more complete and general coverage of this subject, see, for example, [Chr02, Gri02, Grö00].

A *Gabor* (or *Weyl-Heisenberg*) system with *window* g and *lattice constants* $\boldsymbol{a}$ and $\boldsymbol{b}$ is the sequence $(g_{\boldsymbol{q},\boldsymbol{r}})_{\boldsymbol{q},\boldsymbol{r}\in\mathbb{Z}^d}$ of translated and modulated functions

$$g_{\boldsymbol{q},\boldsymbol{r}} \stackrel{\text{def}}{=} T_{\boldsymbol{r}\boldsymbol{a}}M_{\boldsymbol{q}\boldsymbol{b}}g = \mathrm{e}^{\mathrm{i}2\pi\langle \boldsymbol{q}\boldsymbol{b}, \boldsymbol{x}-\boldsymbol{r}\boldsymbol{a}\rangle}g(\boldsymbol{x}-\boldsymbol{r}\boldsymbol{a}).$$

The corresponding *synthesis* or *reconstruction operator*

$$R_g\colon l^2 \to L^2, \qquad R_g c \stackrel{\text{def}}{=} \sum_{\boldsymbol{q},\boldsymbol{r}\in\mathbb{Z}^d} c_{\boldsymbol{q},\boldsymbol{r}}g_{\boldsymbol{q},\boldsymbol{r}}$$

is defined with convergence in the L^2-norm if and only if its adjoint, the so-called *analysis operator*

$$R_g^*\colon L^2 \to l^2, \qquad R_g^* f = \left(\langle f, g_{\boldsymbol{q},\boldsymbol{r}}\rangle\right)_{\boldsymbol{q},\boldsymbol{r}\in\mathbb{Z}^d},$$

is bounded, i.e., if and only if $\sum_{\boldsymbol{q},\boldsymbol{r}\in\mathbb{Z}^d} |\langle f, g_{\boldsymbol{q},\boldsymbol{r}}\rangle|^2 \le B \|f\|_2^2$ for some $B \in \mathbb{R}_+$ and all $f \in L^2(\mathbb{R}^d)$ [Gri02, p. 14].

We call $(g_{\boldsymbol{q},\boldsymbol{r}})_{\boldsymbol{q},\boldsymbol{r}\in\mathbb{Z}^d}$ a Gabor *frame* for $L^2(\mathbb{R}^d)$ if there are *frame bounds* $A, B \in \mathbb{R}_+$ such that for all $f \in L^2(\mathbb{R}^d)$,

$$A\|f\|_2^2 \le \left\|R_g^* f\right\|_2^2 \le B\|f\|_2^2. \tag{2.4}$$

It follows from (2.4) that the *frame operator* $S_g \overset{\text{def}}{=} R_g R_g^*$ is invertible. We call a frame with elements $\widetilde{g}_{\boldsymbol{q},\boldsymbol{r}} \overset{\text{def}}{=} T_{\boldsymbol{r}\boldsymbol{a}} M_{\boldsymbol{q}\boldsymbol{b}} \widetilde{g}$ a *dual Gabor frame* if for every $f \in L^2$,

$$f = \sum_{\boldsymbol{q},\boldsymbol{r}\in\mathbb{Z}^d} \langle f, \widetilde{g}_{\boldsymbol{q},\boldsymbol{r}}\rangle\, g_{\boldsymbol{q},\boldsymbol{r}} = \sum_{\boldsymbol{q},\boldsymbol{r}\in\mathbb{Z}^d} \langle f, g_{\boldsymbol{q},\boldsymbol{r}}\rangle\, \widetilde{g}_{\boldsymbol{q},\boldsymbol{r}} \tag{2.5}$$

with L^2-norm convergence of both series. There may exist (infinitely) many different dual windows $\widetilde{g}$ for g. However, we shall always consider the *canonical dual window*, which is the minimum L^2–norm dual window [Jan98, p. 51]. The dual frame has frame bounds A^{-1}, B^{-1} and the coefficients in (2.5) are not unique in l^2, but they are the unique minimum l^2-norm coefficients. It follows also from (2.4) and (2.5) that $R_{\widetilde{g}}^*$ picks coefficients from $C_{\widetilde{g}} \overset{\text{def}}{=} R_{\widetilde{g}}^*(L^2(\mathbb{R}^d)) \subseteq l^2$ and that R_g is a bounded invertible mapping of $C_{\widetilde{g}}$ onto L^2 with bounded inverse $R_g^{-1} = R_{\widetilde{g}}^*$. By this isomorphism and the usual definition of operator norms we can use two Gabor frames $(g_{\boldsymbol{q},\boldsymbol{r}})$ and $(\gamma_{\boldsymbol{q},\boldsymbol{r}})$ (possibly with different lattice constants) to obtain an isomorphism of the family of linear bounded operators $H\colon L^2(\mathbb{R}^d) \to L^2(\mathbb{R}^d)$ with the coefficient mappings $G = R_\gamma^* H R_g$, as illustrated in the following commutative diagram.

$$\begin{array}{ccc} L^2(\mathbb{R}^d) & \xrightarrow{H} & L^2(\mathbb{R}^d) \\ \uparrow{\scriptstyle R_g} & & \downarrow{\scriptstyle R_\gamma^*} \\ C_{\widetilde{g}} & \xrightarrow{G=R_\gamma^* H R_g} & C_\gamma \end{array} \tag{2.6}$$

We will provide an explicit expression for G in Section 4.

The frame $(g_{\boldsymbol{q},\boldsymbol{r}})_{\boldsymbol{q},\boldsymbol{r}\in\mathbb{Z}^d}$ is called a *Riesz basis* if $C_{\widetilde{g}} = l^2$. Then, the coefficients in (2.5) are truly unique and, as a consequence, $(g_{\boldsymbol{q},\boldsymbol{r}})$ and $(\widetilde{g}_{\boldsymbol{q},\boldsymbol{r}})$ are biorthogonal.

2.4 Hilbert–Schmidt operators

The mathematical framework for the use of Hilbert–Schmidt operators acting on functions defined on locally compact abelian groups has been developed in great generality in harmonic and functional analysis [FK98]. For the basic theory, see, for example, [Con00, RS80] or [Fol95, Appendix 2].

We will use the following classification of Hilbert-Schmidt operators, which is equivalent to the classical definition (see [GP05] or [RS80, Theorem VI.23] for details).

Theorem 2. *A linear bounded operator $H\colon L^2(\mathbb{R}^d) \to L^2(\mathbb{R}^d)$ is Hilbert–Schmidt if and only if there is a function $S_H \in L^2(\mathbb{R}^d \times \mathbb{R}^d)$ such that for all $s \in L^2(\mathbb{R}^d)$,*

$$(Hs)(\boldsymbol{t_0}) = \int_{\mathbb{R}^d \times \mathbb{R}^d} S_H(\boldsymbol{\nu}, \boldsymbol{t}) s(\boldsymbol{t_0} - \boldsymbol{t}) \mathrm{e}^{\mathrm{i}2\pi\langle \boldsymbol{\nu}, \boldsymbol{t_0} - \boldsymbol{t}\rangle}\, d(\boldsymbol{t}, \boldsymbol{\nu}). \tag{2.7}$$

The integral in (2.7) is defined in a weak sense. In fact, for $s, g \in L^2(\mathbb{R}^d)$, we have $g(\cdot)s(\cdot - \boldsymbol{t}) \in L^1$, so that the *short-time Fourier transform* of g with window s is well-defined as the function

$$\mathcal{V}_s g(\boldsymbol{\nu}, \boldsymbol{t}) \stackrel{\text{def}}{=} \int_{\mathbb{R}^d} g(\boldsymbol{t_0}) \overline{s(\boldsymbol{t_0} - \boldsymbol{t})} \mathrm{e}^{-\mathrm{i}2\pi\langle \boldsymbol{\nu}, \boldsymbol{t_0} - \boldsymbol{t}\rangle}\, \mathrm{d}\boldsymbol{t_0} \tag{2.8}$$

on $L^2(\mathbb{R}^d \times \mathbb{R}^d)$. Hence, Hs is defined to be the unique $L^2(\mathbb{R}^d)$-function with

$$\langle Hs, g\rangle_{L^2(\mathbb{R}^d)} = \langle S_H, \mathcal{V}_s g\rangle_{L^2(\mathbb{R}^d \times \mathbb{R}^d)}.$$

There are many similar versions of Theorem 2, some of which can be obtained by applying partial Fourier transforms to S_H and replacing (2.7) with corresponding mappings relating s or $\widehat{s}$ to either Hs or $\widehat{Hs}$ as done in (2.9) below. Many so obtained system functions are known under a rich plethora of different names in the literature, ranging back to a first systematic study by Zadeh and Bello [Zad50, Bel63, Bel64] (see also [Ric03] for an overview). The integral representations of importance in this text describe H in terms of the *spreading function* S_H, the *kernel* κ_H, the *time-varying impulse response* h, the *Kohn-Nirenberg symbol* σ_H and the *bifrequency function* B_H. These system functions are related via the following partial Fourier transforms:

$$\begin{array}{ccc} \kappa_H(\boldsymbol{t_0}, \boldsymbol{t_0} - \boldsymbol{t}) = h(\boldsymbol{t_0}, \boldsymbol{t}) & \overset{\mathcal{F}_{\boldsymbol{t}\to\boldsymbol{\xi}}}{\longmapsto} & \sigma_H(\boldsymbol{t_0}, \boldsymbol{\xi}) \\ \Big\downarrow \mathcal{F}_{\boldsymbol{t_0}\to\boldsymbol{\nu}} & & \Big\downarrow \mathcal{F}_{\boldsymbol{t_0}\to\boldsymbol{\nu}} \\ \mathrm{e}^{-\mathrm{i}2\pi\langle \boldsymbol{\nu}, \boldsymbol{t}\rangle} S_H(\boldsymbol{\nu}, \boldsymbol{t}) & \overset{\mathcal{F}_{\boldsymbol{t}\to\boldsymbol{\xi}}}{\longmapsto} & B_H(\boldsymbol{\nu}, \boldsymbol{\xi}) \end{array} \tag{2.9a}$$

For κ_H being smooth and compactly supported, we apply the Fubini–Tonelli theorem, (2.9a) and Plancherel's theorem to (2.7) to get

$$\begin{aligned} (Hs)(\boldsymbol{t_0}) &= \int \kappa_H(\boldsymbol{t_0}, \boldsymbol{t}) s(\boldsymbol{t})\, \mathrm{d}\mu(\boldsymbol{t}) \\ &= \int_{\mathbb{R}^d} \int_{\mathbb{R}^d} S_H(\boldsymbol{\nu}, \boldsymbol{t}) \mathrm{e}^{\mathrm{i}2\pi\langle \boldsymbol{\nu}, \boldsymbol{x} - \boldsymbol{t}\rangle} d\boldsymbol{\nu} s(\boldsymbol{t_0} - \boldsymbol{t})\, \mathrm{d}\boldsymbol{t} && \text{(2.9b)} \\ &= \int_{\mathbb{R}^d} h(\boldsymbol{t_0}, \boldsymbol{t}) s(\boldsymbol{t_0} - \boldsymbol{t})\, \mathrm{d}\boldsymbol{t} && \text{(2.9c)} \\ &= \int_{\mathbb{R}^d} \sigma_H(\boldsymbol{t_0}, \boldsymbol{\xi}) \widehat{s}(\boldsymbol{\xi}) \mathrm{e}^{\mathrm{i}2\pi\langle \boldsymbol{t_0}, \boldsymbol{\xi}\rangle}\, \mathrm{d}\boldsymbol{\xi} && \text{(2.9d)} \\ &= \int_{\mathbb{R}^d} \int_{\mathbb{R}^d} B_H(\boldsymbol{\nu} - \boldsymbol{\xi}, \boldsymbol{\xi}) \widehat{s}(\boldsymbol{\xi})\, \mathrm{d}\boldsymbol{\xi} \mathrm{e}^{\mathrm{i}2\pi\langle \boldsymbol{t_0}, \boldsymbol{\nu}\rangle}\, \mathrm{d}\boldsymbol{\nu}. \end{aligned}$$

Note that the validity above extends to general Hilbert–Schmidt operators via a density argument. Certainly, the convergence of the integrals is considered in the

L^2 sense as generally done in L^2-Fourier analysis. In this case, the equalities above hold for almost every $\boldsymbol{t_0}$.

It follows naturally from (2.9) to view $h(\boldsymbol{t_0}, \boldsymbol{t})$ as the impulse response at $\boldsymbol{t_0}$ to an impulse at $\boldsymbol{t_0} - \boldsymbol{t}$ and to view $\sigma_H(\boldsymbol{t_0}, \boldsymbol{\xi})$ as the frequency response at $\boldsymbol{t_0}$ to a complex exponential with frequency $\boldsymbol{\xi}$.

A Hilbert–Schmidt operator H is usually called *underspread* if its spreading function is contained in a rectangle with area less than one and *overspread* otherwise. Underspread operators have the important property that they are *identifiable* [KP06, PW05], which means that the operator H can be computed from its response to a selected single input function. The most well-known example of identifiability is the fact that linear time-invariant channels are completely characterized by their action on a Dirac delta distribution, that is, by their impulse response.

3 The channel model

An important and uniting property for radio and sonar communications in air and water, respectively, is *multipath propagation*, which means that due to reflections on different structures in the environment, the transmitted signal reaches the receiver via a possibly infinite number of different wave propagation paths, as illustrated in Figure 2 (see, for example, [Rap02]).

In Sections 3.1–3.2, we examine the multipath propagation model at some depth under the standard assumptions that the electric field component at the receiver is the superposition of the contributions from all signal paths leading there, and that the action of the channel on a transmitted signal is the superposition of the action on all complex exponentials in a Fourier expansion of the signal. For this we use a standard and straightforward linear extension ($H(u + \mathrm{i}v) = Hu + \mathrm{i}Hv$) of H to complex valued functions. Initially, we do also allow the channel to be of infinite lifelength, which is necessary for our class of modelled channels to include, for example, the identity operator, which has a Dirac delta distribution spreading function.

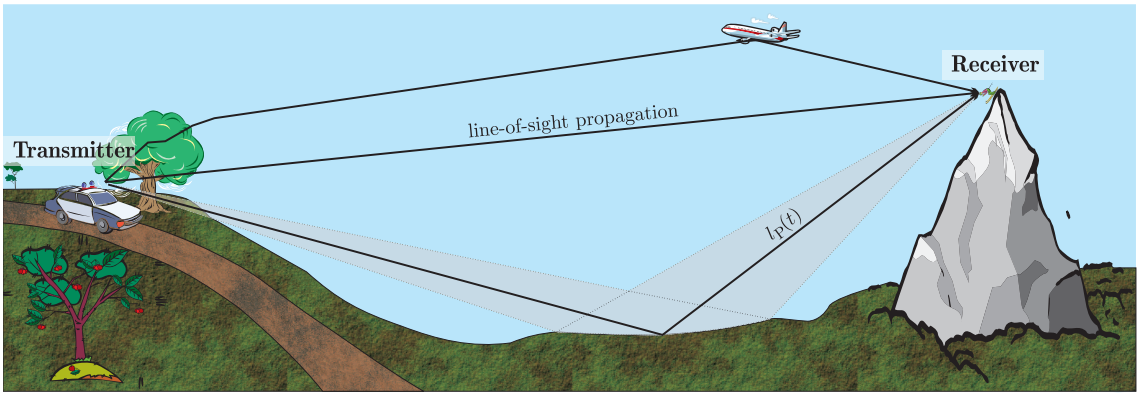

Figure 2: The transmitted signal reaches the receiver along a continuum of different signal paths. Each path P has time-varying length $l_P(t)$.

For communications applications, however, only finite lifelength channels are important. We show in Section 3.3 that this subclass of channels can be completely described by very smooth spreading functions with "essentially compact" support.

3.1 Single path frequency response

Most wireless communication channels change their characteristics slowly compared to the rate at which transmission symbols are sent. Significant changes either require a long time-period to evolve, or they are caused by abrupt changes in the environment, for example, when a mobile telephone user drives into a tunnel. The standard countermeasure is to regularly make new estimates of the channel. In OFDM based methods this is usually done by sending pilot symbols, pilot tones or scattered pilots [GHS+01]. For a more general treatment, see [GHS+01, KP06, LPW05, MMH+02, PW05].

Thus, from now on we shall only consider the *short-time behaviour* of the channel during time intervals I that are short enough to assume a fixed collection of signal paths with the length $l_{\mathrm{P}}(t)$ of path P being a linear function of the time. That is, we assume the length and prolongation-speed of each path to be such that for some $T_0 \in I$ and all $t \in I$,

$$l_{\mathrm{P}}(t) = L_{\mathrm{P}} + V_{\mathrm{P}} \cdot (t - T_0) \qquad \text{with} \qquad |V_{\mathrm{P}} \cdot (t - T_0)| \ll L_{\mathrm{P}}. \tag{3.1}$$

Physical constraints on the speed of antenna and reflecting object movements give some upper bound $V_{\max}$ for $|V_{\mathrm{P}}|$. We will assume $V_{\max}$ to be smaller than the *wave propagation speed* V_{w}, so that

$$V_{\mathrm{w}} > V_{\max} \geq |V_{\mathrm{P}}| \quad \text{for all paths P.}$$

Hence, if a simple harmonic $\mathrm{e}^{\mathrm{i}2\pi\xi t}$ is sent along the path P without any attenuation or perturbations, then the received signal would be

$$\mathrm{e}^{\mathrm{i}2\pi\xi\left(t-\frac{l_{\mathrm{P}}(t)}{V_{\mathrm{w}}}\right)} = \mathrm{e}^{\mathrm{i}2\pi\xi\left(\left(1-\frac{V_{\mathrm{P}}}{V_{\mathrm{w}}}\right)t-\frac{L_{\mathrm{P}}-V_{\mathrm{P}}T_0}{V_{\mathrm{w}}}\right)} = \mathrm{e}^{\mathrm{i}2\pi\xi\left(1-\frac{V_{\mathrm{P}}}{V_{\mathrm{w}}}\right)\left(t-\frac{L_{\mathrm{P}}-V_{\mathrm{P}}T_0}{V_{\mathrm{w}}-V_{\mathrm{P}}}\right)} = T_{t_{\mathrm{P}}} M_{\nu_{\mathrm{P}}\xi} \mathrm{e}^{\mathrm{i}2\pi\xi(\cdot)} \tag{3.2a}$$

where the time and frequency shifts t_{P} and $\nu_{\mathrm{P}}\xi$ satisfy

$$t_{\mathrm{P}} = \frac{L_{\mathrm{P}} - V_{\mathrm{P}}T_0}{V_{\mathrm{w}} - V_{\mathrm{P}}} \quad \text{and} \quad \nu_{\mathrm{P}} = -\frac{V_{\mathrm{P}}}{V_{\mathrm{w}}} \in \left[-\frac{V_{\max}}{V_{\mathrm{w}}}, \frac{V_{\max}}{V_{\mathrm{w}}}\right] \subset (-1, 1). \tag{3.2b}$$

This mapping from $(V_{\mathrm{P}}, L_{\mathrm{P}})$ to $(\nu_{\mathrm{P}}, t_{\mathrm{P}})$ is invertible with inverse

$$V_{\mathrm{P}} = -\nu_{\mathrm{P}} V_{\mathrm{w}} \qquad \text{and} \qquad L_{\mathrm{P}} = V_{\mathrm{w}} \left(t_{\mathrm{P}} \left(1 + \nu_{\mathrm{P}}\right) - \nu_{\mathrm{P}} T_0\right). \tag{3.2c}$$

By (3.2b), (3.1) and (3.2c), there is a compact set $K \subset (-1, 1)$ and some $A \in \mathbb{R}$ such that $(\nu_{\mathrm{P}}, t_{\mathrm{P}}) \in K \times [A, \infty)$ for all paths P.

Now fix some arbitrary $(\nu, t) \in K \times [A, \infty)$ and some path P with frequency response parameters $(\nu_{\mathrm{P}}, t_{\mathrm{P}}) = (\nu, t)$ in (3.2a). The channel operator action on a complex exponential $s_\xi(t_0) = \mathrm{e}^{\mathrm{i}2\pi\xi t_0}$ consists of the following components:

1. A multiplication by a transmitter amplitude gain $G_{\mathrm{T}}(\mathrm{P})$.

   If we identify the path with the angular direction in which it leaves the transmitter, then we can integrate (or sum) over all P and note that for energy conservation reasons the total power gain $\int |G_{\mathrm{T}}(\mathrm{P})|^2 \,\mathrm{dP}$ must be finite.

2. The time-frequency shift by $(\nu_{\mathrm{P}}\xi, t_{\mathrm{P}})$ that is given in (3.2a).

3. Attenuation with a factor[2] $A_\xi(\mathrm{P}) \in \mathbb{R}$ that for free space transmission has size $\mathcal{O}(L_{\mathrm{P}}^{-2})$ for large L_{P} [Rap02, Reu74].

   However, the decay is usually much faster and exponential decay $\mathcal{O}(\mathrm{e}^{-a_\xi L_{\mathrm{P}}})$ can be argued for if we assume some fixed minimum attenuation every time a signal is reflected [Str05]. Even for radio signals propagating through the atmosphere without reflections (*line-of-sight propagation*, see Figure 2), frequency selective absorption causes exponential decay with faster decay for higher frequencies [Reu74, Section 2.1.7]. From this and (3.2c) we get that for some $a_\xi, C > 0$,

   $$|A_\xi(\mathrm{P})| \leq C\mathrm{e}^{-a_\xi L_{\mathrm{P}}} \leq C_\xi \mathrm{e}^{-\alpha t_{\mathrm{P}}} \chi_{[A,\infty)}(t_{\mathrm{P}}) \tag{3.3}$$

   with $C_\xi = \sup_{|\nu|<1} C\mathrm{e}^{a_\xi V_{\mathrm{w}} \nu T_0} < C\mathrm{e}^{a_\xi V_{\mathrm{w}} |T_0|}$ and $\alpha = \inf_\xi \inf_{|\nu|<1} a_\xi V_{\mathrm{w}}(1-\nu) > 0$.

4. Multiplication by a receiver amplitude gain $G_{\mathrm{R}}(\mathrm{P})$, which for any kind of practical use must also satisfy that $\int |G_{\mathrm{R}}(\mathrm{P})|^2 \,\mathrm{dP} < \infty$.

Altogether, the above steps add up to the following single path frequency response:

$$\begin{aligned} s_\xi(\cdot) &\stackrel{\mathrm{def}}{=} \mathrm{e}^{\mathrm{i}2\pi\xi(\cdot)} \xrightarrow{\text{Transmitter}} G_{\mathrm{T}}(\mathrm{P}) s_\xi \\ &\xrightarrow{\text{TF-shift (3.2a)}} G_{\mathrm{T}}(\mathrm{P}) T_{t_{\mathrm{P}}} M_{\nu_{\mathrm{P}}\xi} s_\xi \\ &\xrightarrow{\text{Attenuation}} G_{\mathrm{T}}(\mathrm{P}) A_\xi(\mathrm{P}) T_{t_{\mathrm{P}}} M_{\nu_{\mathrm{P}}\xi} s_\xi \\ &\xrightarrow{\text{Receiver}} G_{\mathrm{T}}(\mathrm{P}) A_\xi(\mathrm{P}) G_{\mathrm{R}}(\mathrm{P}) T_{t_{\mathrm{P}}} M_{\nu_{\mathrm{P}}\xi} s_\xi \end{aligned} \tag{3.4}$$

Now set

$$B_\xi(\mathrm{P}) \stackrel{\mathrm{def}}{=} A_\xi(\mathrm{P}) \mathrm{e}^{\alpha_\xi t_{\mathrm{P}}}$$

for all paths P, so that by (3.3), $|B_\xi(\mathrm{P})| \leq C_\xi$ for all P. Further, we set $P_{\nu,t} = \{\mathrm{P} : (\nu_{\mathrm{P}}, t_{\mathrm{P}}) = (\nu, t)\}$.

As usual for electromagnetic waves, we expect the electric field component measured at the receiver to be the superposition of the electric field components received from the different paths P (and similarly for sonar waves), or written as a formal integration[3]

$$(Hs_\xi)(t_0) = \int_{K\times[A,\infty)} \left(\int_{P_{\nu,t}} G_{\mathrm{T}}(\mathrm{P}) B_\xi(\mathrm{P}) G_{\mathrm{R}}(\mathrm{P}) \,\mathrm{dP} \right) \mathrm{e}^{-\alpha_\xi t} (T_t M_{\nu\xi} s_\xi)(t_0) \,\mathrm{d}(\nu, t). \tag{3.5}$$

[2]We allow $A_\xi(\mathrm{P})$ to be negative to include potential sign-changes caused by reflections.

[3]Here again, $\int \cdots \mathrm{dP}$ is shorthand notation for the integration over the different angles in a polar coordinate system.

If we denote the inner integral

$$r_\xi(\nu,t) \stackrel{\text{def}}{=} \int_{P_{\nu,t}} G_{\mathrm{T}}(\mathrm{P})B_\xi(\mathrm{P})G_{\mathrm{R}}(\mathrm{P})\,\mathrm{dP}, \tag{3.6a}$$

then it follows from the Hölder inequality, the bound $|B_\xi(\mathrm{P})| \le C_\xi$ and items 1 and 4 above that

$$\begin{aligned}\int_{K\times[A,\infty)} |r_\xi(\nu,t)|\,\mathrm{d}(\nu,t) \le& \int_{\cup_{(\nu,t)\in K\times[A,\infty)}P_{(\nu,t)}} |G_{\mathrm{T}}(\mathrm{P})B_\xi(\mathrm{P})G_{\mathrm{R}}(\mathrm{P})|\,\mathrm{dP}\\ \le& C_\xi\cdot\|G_{\mathrm{T}}\|_2\cdot\|G_{\mathrm{R}}\|_2<\infty.\end{aligned} \tag{3.6b}$$

Both for the actual transmitted real-valued signals and for our linear extension of H to complex-valued signals, the gain and attenuation factors are all real-valued. We shall however, without any extra effort, allow for complex-valued r in our mathematical model. Moreover, for inclusion of some important idealized borderline cases such as r being a Dirac delta distribution, and for avoiding some computational distribution theory technicalities, we choose to model the integrals $\rho_\xi(U\times V) \stackrel{\text{def}}{=} \int_{U\times V} r_\xi(\nu,t)\,\mathrm{d}(\nu,t)$ over sets $U\times V \subseteq K\times[A,\infty)$ to be a complex Borel measure ρ_ξ with finite total variation, that is

$$\rho_\xi(U\times V) = \int_{U\times V} \mathrm{d}\rho_\xi(\nu,t) \qquad \text{with} \qquad |\rho_\xi|\,(K\times[A,\infty)) < \infty. \tag{3.7a}$$

Thus, in this mathematical model, (3.5) takes the form

$$(Hs_\xi)(t_0) = \int_{K\times[A,\infty)} \mathrm{e}^{-\alpha_\xi t}(T_t M_{\nu_\xi} s_\xi)(t_0)\,\mathrm{d}\rho_\xi(\nu,t). \tag{3.7b}$$

Note that this model includes, for example, Dirac measures and thus also the identity operator.

3.2 Narrowband signals

We shall call the transmitted signal s *narrowband* if $\widehat{s}$ is well-localized enough to justify the approximations

$$\nu\xi \approx \nu\xi_0, \qquad \mathrm{e}^{-\alpha_\xi t} \approx \mathrm{e}^{-\alpha_{\xi_0} t} \qquad \text{and} \qquad \rho_\xi \approx \rho_{\xi_0} \tag{3.8}$$

in the computations leading to (3.9b) below. We will primarily assume this narrowband assumption to hold for the same ξ_0 in the entire transmission frequency band. In the remark on page 26, we will show that this assumption holds true for some radio communications examples and discuss a refined model with different ξ_0 for different basis functions that is necessary in underwater sonar communications.

Suppose now that the physical channel has the property that its action on a signal s is the superposition of its action on each complex exponential in a Fourier expansion of s, that is,

$$Hs(\cdot) = H\int_{\mathbb{R}} \widehat{s}(\xi)\mathrm{e}^{\mathrm{i}2\pi\xi(\cdot)}\,\mathrm{d}\xi = \int_{\mathbb{R}} \widehat{s}(\xi)H\mathrm{e}^{\mathrm{i}2\pi\xi(\cdot)}\,\mathrm{d}\xi. \tag{3.9a}$$

Then, at least for bandlimited and thus continuous narrowband L^1-signals s, we can apply (3.7b), (3.8) and the Fubini–Tonelli theorem to obtain

$$\begin{aligned}
Hs(t_0) &= \int_{\mathbb{R}} \widehat{s}(\xi) \int_{K\times[A,\infty)} \mathrm{e}^{-\alpha_\xi t}\mathrm{e}^{\mathrm{i}2\pi\nu\xi(t_0-t)}\mathrm{e}^{\mathrm{i}2\pi\xi(t_0-t)}\,\mathrm{d}\rho_\xi(\nu,t)\,\mathrm{d}\xi \\
&\approx \int_{\mathbb{R}} \widehat{s}(\xi) \int_{K\times[A,\infty)} \mathrm{e}^{-\alpha_{\xi_0} t}\mathrm{e}^{\mathrm{i}2\pi\nu\xi_0(t_0-t)}\mathrm{e}^{\mathrm{i}2\pi\xi(t_0-t)}\,\mathrm{d}\rho_{\xi_0}(\nu,t)\,\mathrm{d}\xi \\
&= \int_{K\times[A,\infty)} \mathrm{e}^{-\alpha_{\xi_0} t}\mathrm{e}^{\mathrm{i}2\pi\nu\xi_0(t_0-t)} \int_{\mathbb{R}} \widehat{s}(\xi)\mathrm{e}^{\mathrm{i}2\pi\xi(t_0-t)}\,\mathrm{d}\xi\,\mathrm{d}\rho_{\xi_0}(\nu,t) \\
&= \int_{K\times[A,\infty)} \mathrm{e}^{-\alpha_{\xi_0} t}\mathrm{e}^{\mathrm{i}2\pi\nu\xi_0(t_0-t)} s(t_0-t)\,\mathrm{d}\rho_{\xi_0}(\nu,t).
\end{aligned}$$

We use the last expression as definition of our mathematical model

$$Hs(t_0) \stackrel{\text{def}}{=} \int_{K\times[A,\infty)} \mathrm{e}^{-\alpha_{\xi_0} t}(T_t M_{\nu\xi_0} s)(t_0)\,\mathrm{d}\rho_{\xi_0}(\nu,t). \tag{3.9b}$$

If $s \in L^2(\mathbb{R})$, then by (3.9b) and the Minkowski integral inequality

$$\begin{aligned}
\|Hs\|_2 &= \left\| \int_{K\times[A,\infty)} \mathrm{e}^{-\alpha_{\xi_0} t}(T_t M_{\nu\xi_0} s)(\cdot)\,\mathrm{d}\rho_{\xi_0}(\nu,t) \right\|_2 \\
&\le \int_{K\times[A,\infty)} \mathrm{e}^{-\alpha_{\xi_0} t}\,\|T_t M_{\nu\xi_0} s\|_2\,\mathrm{d}\,|\rho_{\xi_0}|\,(\nu,t) \\
&\le |\rho_{\xi_0}|\,(K\times[A,\infty))\mathrm{e}^{-\alpha_{\xi_0} A}\,\|s\|_2\,.
\end{aligned}$$

Hence equation (3.9b) defines a bounded linear mapping $H\colon L^2(\mathbb{R}) \to L^2(\mathbb{R})$. If, in addition, ρ_{ξ_0} is absolutely continuous with respect to the Lebesgue measure, then we can write $\mathrm{d}\rho_{\xi_0}(\nu,t) = r_{\xi_0}(\nu,t)\,\mathrm{d}(\nu,t)$ where r_{ξ_0} is the function in (3.6), which equals the inner integral in our physical model (3.5). In practice, r_{ξ_0} will be bounded and thus also in $L^2(\mathbb{R})$. Application of this to (3.9b) and the substitution $\nu' = \nu\xi_0$ gives

$$\begin{aligned}
Hs(\cdot) &= \int_{K'\times[A,\infty)} S_H(\nu',t)(T_t M_{\nu'} s)(\cdot)\,\mathrm{d}(\nu',t), \qquad K' \subseteq (-\xi_0,\xi_0) \text{ compact}, \\
S_H(\nu',t) &\stackrel{\text{def}}{=} \frac{1}{\xi_0} r_{\xi_0}\left(\frac{\nu'}{\xi_0},t\right)\mathrm{e}^{-\alpha_{\xi_0} t}\chi_{K'\times[A,\infty)}(\nu',t) \qquad \text{and} \qquad r_{\xi_0} \in L^1 \cap L^2(\mathbb{R}\times\mathbb{R}).
\end{aligned} \tag{3.9c}$$

Alternatively we can use (3.9b) as the definition of a larger space of operators on a smaller space of functions by allowing a larger subclass of the complex Borel measures, such as, the class of all complex Borel measures ρ_{ξ_0} for which the mapping

$$\varphi \mapsto \int_{K\times[A,\infty)} \varphi(\nu,t)\mathrm{e}^{-\alpha_{\xi_0} t}\,\mathrm{d}\rho_{\xi_0}(\nu,t)$$

defines a linear bounded functional S_H on $S_0(K\times[A,\infty))$. Then for all functions s for which the mapping

$$(\nu\xi_0,t) \mapsto (T_t M_{\nu\xi_0} s)(t_0) \in S_0(K'\times[A,\infty)) \qquad \text{for all } t_0, \tag{3.10}$$

is well-defined, it follows that (3.9b) is pointwise well-defined for all t_0. Consequently (3.9b) can be interpreted as the application of a functional $S_H \in S_0'$ to the test function (3.10), or, with the usual formal integral notation,

$$Hs(\cdot) = \int_{K' \times [A,\infty)} S_H(\nu', t)(T_t M_{\nu'} s)(\cdot)\, \mathrm{d}(\nu', t), \qquad S_H \in S_0'(K' \times [A, \infty)).$$

Since the space $S_0'(\mathbb{R} \times \mathbb{R})$ includes Dirac delta distributions, this model includes important idealized borderline cases such as the following:

Line-of-sight transmission: $S_H = a\delta_{\nu_0,t_0}$, a Dirac distribution at (ν_0, t_0) representing a time- and Doppler-shift with attenuation a.

Time-invariant systems: $h(x,t) = h(0,t)$ and $S_H(\nu, t) = h(t)\delta_0(\nu)$.

Moreover, S_0' excludes derivatives of Dirac distributions, which can be used to avoid complex-valued Hs with no physical meaning [Ric03, Sec. 3.1.1]. Further, S_0 is the smallest Banach space of test functions with some useful properties like invariance under time-frequency shifts [Grö00, p.253], thus allowing for time-frequency analysis on its dual S_0' which is, in that particular sense, the largest possible Banach space of tempered distributions that is useful for time-frequency analysis. One more motivation for considering spreading functions in S_0' is that Hilbert–Schmidt operators are compact, hence, they exclude invertible operators, such as the example $S_H = a\delta_{\nu_0,t_0}$ above, and small perturbations of invertible operators, which are useful in the theory of radar identification and in some mobile communication applications. For results using a Banach space setup, see for example [PW05, Str05].

Therefore it may come as a surprise that we will show in Section 3.3 that the Hilbert–Schmidt model (3.9c) is a natural choice for wireless communications channels. This also justifies our use of this model in the remaining paper.

3.3 Finite lifelength channels

We shall show that wireless communications channels can be modelled well by well-localized C^∞-spreading functions. This fact allows for a minimal use of distribution theory in our analysis and adds simplicity to proofs, results and software development both in this paper and for mathematical and numerical analysis of wireless communications channels in general.

In the following, we will assume that the bifrequency function

$$B_H(\nu, \cdot) \text{ is compactly supported.} \tag{3.11}$$

This is not strictly true in general, but we will find that for the narrowband signals $s = g_{\boldsymbol{q},\boldsymbol{r}}$ that we consider, Hs will only depend on the restriction of $B_H(\nu, \cdot)$ to a certain compact interval, so that we are free to set it equal to zero outside that interval (see Figure 5 and the discussion before (4.13a)). Moreover, recall from (3.9c) that $S_H(\cdot, t)$ has compact support as well. Hence, combining this with (2.9a) and (3.11), we see that the distribution $B_H(\nu, \xi)$ is compactly supported. Consequently, since

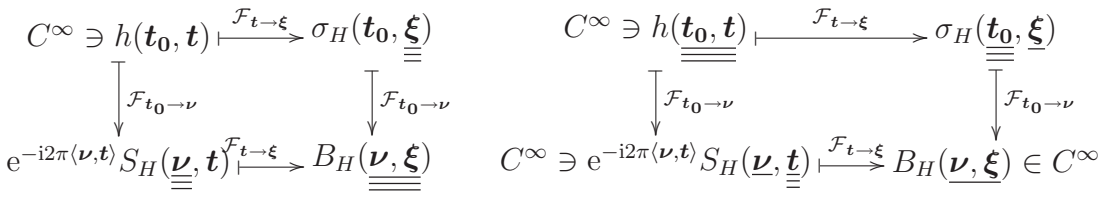

Figure 3: (a) Bandlimiting properties of the physical channel provides us with compactly supported B_H. Thus $h \in C^\infty$, but S_H may be a tempered distribution, for example, if $h(\boldsymbol{t_0},\boldsymbol{t}) = h(\boldsymbol{0},\boldsymbol{t})$. (b) Our restriction to *finite lifelength* channels gives a well localized $S_H \in C^\infty$. In (a) and (b) we denote with underlining subexponential decay, exponential decay and compact support.

the bifrequency function satisfies $B_H = \widehat{h}$, we have that $h \in C^\infty(\mathbb{R}^2)$. We summarize a straightforward generalization of these properties to functions on $\mathbb{R}^d$ in Figure 3 (a).

Since we are modelling the short time input-output relationships of a channel, any useful communications system must be constructed to be independent of the properties of h outside some compact set K_h. Thus, we are free to multiply h with a compactly supported function $w \in C^\infty(\mathbb{R}^{2d})$ such that $w = 1$ on K_h and $\widehat{w}$ is subexponentially decaying (as described in Section 2.2). It is easy to check that it follows from this and from the compact support of $\widehat{h}$ that also the convolution $\widehat{wh} = \widehat{w} * \widehat{h}$ is subexponentially decaying. Now let H_1 be the Hilbert–Schmidt operator with time-varying impulse response $wh \in C^\infty$. From the fact that the space of Schwartz functions is invariant under partial Fourier transforms, it follows that also $S_{H_1} \in C^\infty$. This gives an operator with system function properties that we summarize in the multivariate case in Figure 3 (b). We will also assume that w is chosen to be "wide and smooth enough" so that the smooth cut-off of $S_H(\boldsymbol{\nu},\cdot)$ only deletes a very small-amplitude and negligible part of its exponential tail, and so that also the "blurring out" of the compact support of $S_H(\cdot,\boldsymbol{t})$ to subexponential decay has a rather small impact on the shape of S_H, which therefore can be expected to resemble those given in the Figures of Section 6.

The following sections are devoted to Hilbert–Schmidt operators having exactly the properties described in Figure 3 (b). All results apply directly to the communication channels described in this section as long as the narrowband assumption of Section 3.2 holds for the entire frequency band of the transmitted signals. We describe in a remark on page 26 how refined versions of our results can be applied to wideband signals as long as the attenuation factor A_ξ of (3.3) is roughly frequency independent within the transmission frequency band.

Remark. The exponential decay of $S_H(\nu,\cdot)$ only affects the just mentioned shape of S_{H_1}. In general, the reasoning in this and the following sections hold also with exponential and subexponential decays replaced by other forms of rapid decay.

4 Discretization of the channel model

In this section we derive finite sum formulas for the computation of the matrix representation of the coefficient mapping G in (2.6) for classes of multivariate Hilbert–Schmidt operators H that satisfy the properties summarized in Figure 3 (b).

For the series expansions in Gabor frames $(g_{\boldsymbol{q},\boldsymbol{r}})$ and $(\gamma_{\boldsymbol{q}',\boldsymbol{r}'})$ in Section 2.3, H maps any L^2-function $s = \sum_{\boldsymbol{q},\boldsymbol{r}\in\mathbb{Z}^d} \langle s, \widetilde{g}_{\boldsymbol{q},\boldsymbol{r}}\rangle\, g_{\boldsymbol{q},\boldsymbol{r}}$ to

$$\begin{aligned} Hs &= \sum_{\boldsymbol{q}',\boldsymbol{r}'\in\mathbb{Z}^d} \langle Hs, \gamma_{\boldsymbol{q}',\boldsymbol{r}'}\rangle\, \widetilde{\gamma}_{\boldsymbol{q}',\boldsymbol{r}'} = \sum_{\boldsymbol{q}',\boldsymbol{r}'\in\mathbb{Z}^d} \left\langle H \sum_{\boldsymbol{q},\boldsymbol{r}\in\mathbb{Z}^d} \langle s, \widetilde{g}_{\boldsymbol{q},\boldsymbol{r}}\rangle\, g_{\boldsymbol{q},\boldsymbol{r}}\,, \gamma_{\boldsymbol{q}',\boldsymbol{r}'} \right\rangle \widetilde{\gamma}_{\boldsymbol{q}',\boldsymbol{r}'} \\ &= \sum_{\boldsymbol{q}',\boldsymbol{r}'\in\mathbb{Z}^d} \left(\sum_{\boldsymbol{q},\boldsymbol{r}\in\mathbb{Z}^d} \langle s, \widetilde{g}_{\boldsymbol{q},\boldsymbol{r}}\rangle\, \langle Hg_{\boldsymbol{q},\boldsymbol{r}}, \gamma_{\boldsymbol{q}',\boldsymbol{r}'}\rangle \right) \widetilde{\gamma}_{\boldsymbol{q}',\boldsymbol{r}'}, \end{aligned} \tag{4.1}$$

where convergence in $L^2(\mathbb{R}^d)$ follows from the continuity of H and of the inner product. Thus the coefficient mapping G in (2.6) is

$$G\colon\ (\langle s, \widetilde{g}_{\boldsymbol{q},\boldsymbol{r}}\rangle)_{\boldsymbol{q},\boldsymbol{r}} \mapsto \left(\sum_{\boldsymbol{q},\boldsymbol{r}\in\mathbb{Z}^d} \langle s, \widetilde{g}_{\boldsymbol{q},\boldsymbol{r}}\rangle\, \langle Hg_{\boldsymbol{q},\boldsymbol{r}}, \gamma_{\boldsymbol{q}',\boldsymbol{r}'}\rangle \right)_{\boldsymbol{q}',\boldsymbol{r}'}$$

with biinfinite matrix representation

$$\mathrm{G}_{\boldsymbol{q}',\boldsymbol{r}';\boldsymbol{q},\boldsymbol{r}} = \langle Hg_{\boldsymbol{q},\boldsymbol{r}}, \gamma_{\boldsymbol{q}',\boldsymbol{r}'}\rangle\,, \tag{4.2}$$

and with $2d$-dimensional indices $(\boldsymbol{q}', \boldsymbol{r}')$ and $(\boldsymbol{q}, \boldsymbol{r})$ for rows and columns respectively.

For communications applications with Q carrier frequencies, at least Q samples of every received symbol are needed in the receiver. Thus a hasty and naive approach to computing the matrix elements could start with a $Q \times Q$ matrix representation of H for computing the samples of $Hg_{q,r}$. If every R neighbouring symbols have overlapping ϵ-essential support, then we need to compute $(RQ)^2$ matrix elements $\langle Hg_{q,r}, \gamma_{q',r'}\rangle$, which, with this approach, would require $R^2 \cdot \mathcal{O}(Q^5)$ arithmetic operations with Q typically being at least of the size 256–1024 in radio communications, and with $R = 4$ for $\epsilon = 10^{-6}$ and the optimally well-localized Gaussian windows that we shall use for our example applications in Section 6 (see Figure 12). This is a quite demanding task, so there is a clear need for the more efficient formulas and algorithms that we shall derive in the following sections.

We begin in Section 4.1 with motivating the use of well time-frequency localized Gabor bases. Then, in Section 4.2 we introduce the tools and notation that we find most suitable for discretization of Hilbert-Schmidt operators with the properties summarized in Figure 3 (b). Finally, in Section 4.3 we use these tools for deriving more efficient formulas for computing the matrix elements under a minimum of further assumptions, simplifications or approximations.

Remark. If $(g_{\boldsymbol{q},\boldsymbol{r}})$ is a frame for its closed linear span but not a Riesz basis, then the coefficient subspace $C_{\widetilde{g}}$ of (2.6) will be a proper subspace of l^2. Thus an orthogonal projection to $C_{\widetilde{g}}$ in the receiver would add some stability against noise

and perturbations, but at the cost of an additional requirement on the transmitter to only use coefficient sequences in $C_{\widetilde{g}}$.

For systems in use today, it is typical to instead use Gabor Riesz bases and arbitrary coefficient sequences with coefficients chosen from some standard coefficient constellation, such as quadrature amplitude modulation (QAT), with maximum coefficient amplitude given by transmission power regulations.

4.1 Gabor bases for near-diagonalization

Although (4.1) holds for any pair of frames $(g_{\boldsymbol{i}})$ and $(\gamma_{\boldsymbol{j}})$, Gabor Riesz bases are traditionally used for communications applications. Gabor systems give good diagonalization of G, especially if all basis elements are narrowband (see below and [KPZ02]).

We call an operator H *time-invariant* if it commutes with the translation operator $T_{\boldsymbol{t_0}}$ for any $\boldsymbol{t_0}$, that is, if $T_{\boldsymbol{t_0}}H = HT_{\boldsymbol{t_0}}$. Consequently, the impulse response h of H satisfy $h(\boldsymbol{t_0}, \boldsymbol{t}) = h(\boldsymbol{0}, \boldsymbol{t})$ and (2.9d) becomes a convolution $h(\boldsymbol{0}, \cdot) * s$. Then the family of complex exponentials $\mathrm{e}^{i2\pi\langle\boldsymbol{\xi},\cdot\rangle}$ are "eigenfunctions" in the sense that for inputs of the form $s(\cdot) = \mathrm{e}^{i2\pi\langle\boldsymbol{\xi},\cdot\rangle}\chi_{[\boldsymbol{0},\boldsymbol{L}]}(\cdot)$, there is some complex scalar $\lambda_{\boldsymbol{\xi}}$ such that if $\operatorname{supp} h = [\boldsymbol{0}, \boldsymbol{L_h}]$, then $Hs = \lambda_{\boldsymbol{\xi}} s$ in the interval $[\boldsymbol{L_h}, \boldsymbol{L}]$, as illustrated in Figure 4. Thus G is easily diagonalized by using Gabor windows $g = \chi_{[\boldsymbol{0},\boldsymbol{L}]}$, $\gamma = \chi_{[\boldsymbol{L_h},\boldsymbol{L}]}$ and lattice constants such that the resulting Gabor systems $(g_{\boldsymbol{k},\boldsymbol{l}})$ and $(\gamma_{\boldsymbol{k},\boldsymbol{l}})$ are biorthogonal bases for their respective span. This trick is used in wireline communications, where the smaller support of γ is obtained by removing a guard interval (often called *cyclic prefix*) from g. See, for example, [Gri02, Section 2.3] for more details and further references.

In *wireless* communications, we can at most hope for approximate diagonalization of the channel operator due to its time varying nature. In general, two different time-varying operators do not commute, so both cannot be diagonalized with the same choice of bases. Thus, diagonalization is usually only possible in the following sense: Typically, $(Hg_{\boldsymbol{q},\boldsymbol{r}})$ is a finite and linearly independent sequence, and thus a Riesz basis with some dual basis $\left(\widetilde{Hg_{\boldsymbol{q},\boldsymbol{r}}}\right)$. In fact, since the computations in (4.1) are not restricted to Gabor frames, we can set $\gamma_{\boldsymbol{q'},\boldsymbol{r'}} = \widetilde{Hg_{\boldsymbol{q},\boldsymbol{r}}}$, which gives true diagonalization of (4.2), but in general, $\widetilde{Hg_{\boldsymbol{q},\boldsymbol{r}}}$ will not be a Gabor frame or have any other basic structure that enables efficient computation of all $\widetilde{Hg_{\boldsymbol{q},\boldsymbol{r}}}$ and all the inner products $\left\langle Hg_{\boldsymbol{q},\boldsymbol{r}}, \widetilde{Hg_{\boldsymbol{q'},\boldsymbol{r'}}} \right\rangle$.

Thus, for computational complexity to meet practical restrictions we will use

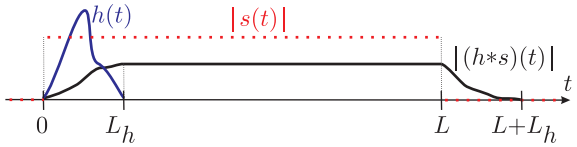

Figure 4: Convolution of a compactly supported complex exponential $s(t) = \chi_{[0,L]}(t)\mathrm{e}^{i2\pi\xi t}$ with a function $h = h\chi_{[0,L_h]}$ will on the interval $[L_h, L]$ equal the same complex exponential multiplied with a complex scalar.

"almost dual" Gabor bases $(g_{\boldsymbol{q},\boldsymbol{r}})$ and $(\gamma_{\boldsymbol{q}',\boldsymbol{r}'})$, such as the Gabor bases proposed in [MSG+05]. We are primarily interested in bases that are good candidates for providing low intersymbol and interchannel interference (ISI and ICI). As proposed in [MSG+05], we expect excellent joint time-frequency concentration of g and γ to be the most important requirement for achieving that goal.

We will strive to customize decisions like the choice of discretization methods for channels with the system function properties summarized in Figure 3 (b) and for windows g and γ that are bandlimited and decay "fast enough" to be represented by a finite (and reasonably small) number of Nyquist frequency samples. This is the topic of sections 4.2 and 4.3.

4.2 Discretization tools

Recall first from Section 3.3 and Figure 3 (b) that it is justified to work with spreading functions that can be truncated to compact support with negligible truncation errors.

Then Proposition 1 below shows that the functions $Hg_{\boldsymbol{q},\boldsymbol{r}}$ and $\widehat{Hg_{\boldsymbol{q},\boldsymbol{r}}}$ are well localized around the lattice points of a lattice with the same lattice constants as the lattice of the Gabor basis $(g_{\boldsymbol{q},\boldsymbol{r}})$. This suggests to choose $(\gamma_{\boldsymbol{q}',\boldsymbol{r}'})$ to be a Gabor basis with the same lattice constants as $(g_{\boldsymbol{q},\boldsymbol{r}})$. For this scenario, propositions 2–4 in Section 4.3 provide us with formulas that allow an efficient computation of the matrix elements $\langle Hg_{\boldsymbol{q},\boldsymbol{r}}, \gamma_{\boldsymbol{q}',\boldsymbol{r}'}\rangle$.

Proposition 1. *Suppose that H is a Hilbert–Schmidt operator on $L^2(\mathbb{R}^d)$,*

$$\operatorname{supp} S_H \subseteq I_{\boldsymbol{\omega}_c,\boldsymbol{\omega}} \times [\boldsymbol{a},\boldsymbol{b}] \qquad \text{and} \qquad g \in L^2(\mathbb{R}^d). \tag{4.3}$$

(a) If $\operatorname{supp} f \subseteq [\boldsymbol{A},\boldsymbol{B}]$, *then* $\operatorname{supp} Hf \subseteq [\boldsymbol{A}+\boldsymbol{a},\boldsymbol{B}+\boldsymbol{b}]$.

(b) If $\operatorname{supp} \widehat{f} \subseteq I_{\boldsymbol{C}_f,\boldsymbol{B}_f}$, *then* $\operatorname{supp} \widehat{Hg} \subseteq I_{\boldsymbol{C}_f+\boldsymbol{\omega}_c,\boldsymbol{B}_f+\boldsymbol{\omega}}$.

The proof of Proposition 1 is rather straightforward and can be found in [GP05].

We will repeatedly apply the following special case of the Poisson Summation formula [Grö00, Kat04] to the functions $g_{\boldsymbol{q},\boldsymbol{r}}$, $Hg_{\boldsymbol{q},\boldsymbol{r}}$ and $\gamma_{\boldsymbol{q}',\boldsymbol{r}'}$:

Theorem 3 (Sampling theorems). *Suppose that $f \in L^2(\mathbb{R}^d)$ has a Fourier transform with support* $\operatorname{supp} \widehat{f} \subseteq I_{\boldsymbol{C}_f,\boldsymbol{B}_f}$. *Then $\widehat{f} \in L^1(\mathbb{R}^d) \cap L^2(\mathbb{R}^d)$, f is continuous (modulo modifications on a set of measure 0) and for all $\boldsymbol{\xi} \in \widehat{\mathbb{R}^d}$,*

$$\widehat{f}(\boldsymbol{\xi}) = |\boldsymbol{T}_f|\, \chi_{I_{\boldsymbol{C}_f,\boldsymbol{B}_f}}(\boldsymbol{\xi}) \sum_{\boldsymbol{k}\in\mathbb{Z}^d} f(\boldsymbol{k}\boldsymbol{T}_f) \mathrm{e}^{-\mathrm{i}2\pi\langle \boldsymbol{\xi}, \boldsymbol{k}\boldsymbol{T}_f\rangle}, \qquad \boldsymbol{T}_f = \frac{\mathbf{1}}{\boldsymbol{B}_f}. \tag{4.4a}$$

Equivalently (via (2.1)*),* (4.4a) *is also known as the* Nyquist sampling theorem

$$f(\boldsymbol{t}) = |\boldsymbol{T}_f| \sum_{\boldsymbol{k}\in\mathbb{Z}^d} f(\boldsymbol{k}\boldsymbol{T}_f) \mathrm{e}^{\mathrm{i}2\pi\langle \boldsymbol{C}_f, \boldsymbol{t}-\boldsymbol{k}\boldsymbol{T}_f\rangle} \operatorname{sinc}_{\boldsymbol{B}_f}(\boldsymbol{t}-\boldsymbol{k}\boldsymbol{T}_f). \tag{4.4b}$$

For $\boldsymbol{a} \in \mathbb{Z}^d$, some $\boldsymbol{b}, \boldsymbol{\Omega} \in \mathbb{R}_+^d$ and f equal to $g_{\boldsymbol{q},\boldsymbol{r}}$ or $\gamma_{\boldsymbol{q}',\boldsymbol{r}'}$, we will consider time-frequency shifts $f_{\boldsymbol{q},\boldsymbol{r}} \stackrel{\text{def}}{=} T_{\boldsymbol{r}\boldsymbol{a}\boldsymbol{T}_g} M_{\boldsymbol{q}\boldsymbol{b}\boldsymbol{\Omega}} f$, for which

$$\boldsymbol{T}_{\boldsymbol{g}} \stackrel{\text{def}}{=} \frac{1}{\boldsymbol{\Omega}}, \qquad \operatorname{supp} \widehat{f_{\boldsymbol{q},\boldsymbol{r}}}, \subseteq I_{\boldsymbol{C}_f + \boldsymbol{q}\boldsymbol{b}\boldsymbol{\Omega}, \boldsymbol{B}_f}, \tag{4.5a}$$

and the Nyquist frequency samples are

$$f_{\boldsymbol{q},\boldsymbol{r}}(\boldsymbol{k}\boldsymbol{T}_{\boldsymbol{f}}) = f(\boldsymbol{k}\boldsymbol{T}_{\boldsymbol{f}} - \boldsymbol{r}\boldsymbol{a}\boldsymbol{T}_{\boldsymbol{g}}) \mathrm{e}^{\mathrm{i}2\pi \langle \boldsymbol{k}\boldsymbol{T}_f - \boldsymbol{r}\boldsymbol{a}\boldsymbol{T}_g, \boldsymbol{q}\boldsymbol{b}\boldsymbol{\Omega} \rangle}. \tag{4.5b}$$

If $\boldsymbol{T}_{\boldsymbol{g}} = \boldsymbol{T}_{\boldsymbol{f}}$, then (4.5b) becomes

$$f_{\boldsymbol{q},\boldsymbol{r}}(\boldsymbol{k}\boldsymbol{T}_{\boldsymbol{g}}) = f((\boldsymbol{k} - \boldsymbol{r}\boldsymbol{a})\boldsymbol{T}_{\boldsymbol{g}}) \mathrm{e}^{\mathrm{i}2\pi \langle \boldsymbol{k} - \boldsymbol{r}\boldsymbol{a}, \boldsymbol{q}\boldsymbol{b} \rangle}.$$

If $\boldsymbol{T}_{\boldsymbol{g}} \neq \boldsymbol{T}_{\boldsymbol{f}}$, then we can instead compute the samples $f(\boldsymbol{k}\boldsymbol{T}_{\boldsymbol{f}} - \boldsymbol{r}\boldsymbol{a}\boldsymbol{T}_{\boldsymbol{g}})$ by applying (4.4b), which will be a finite sum formula for those f that we will consider.

Proposition 1, Theorem 3, (4.5a) and (4.5b) are the basic tools that we will use to compute the matrix elements $\langle H g_{\boldsymbol{q},\boldsymbol{r}}, \gamma_{\boldsymbol{q}',\boldsymbol{r}'} \rangle$. We will apply these to bandlimited g and γ that have only a finite number of nonzero samples in the Nyquist reconstruction formula (4.4b). These samples should be chosen so that g and γ decay fast enough to allow truncation to compact support with both the maximum and the L^2-norm of the truncation error being less than some ϵ well below the overall noise level of the application at hand. In Figure 7 on page 33, we show by example how such window functions can be constructed. For the scenario that we summarized in Figure 3 (b), we can, in practice, regard S_H to be compactly supported and conclude from Proposition 1 that $H g_{\boldsymbol{q},\boldsymbol{r}}$ and $\widehat{H g_{\boldsymbol{q},\boldsymbol{r}}}$ inherits the good localization properties of $g_{\boldsymbol{q},\boldsymbol{r}}$, $\widehat{g_{\boldsymbol{q},\boldsymbol{r}}}$ and S_H. Hence, with negligible truncation errors, we can assume also $H g_{\boldsymbol{q},\boldsymbol{r}}$ to be bandlimited, to be fully described by a finite number of Nyquist frequency samples and to have ϵ-essential time-frequency support given by Proposition 1. (In Section 5 we choose $\epsilon = 10^{-6}$.) Throughout the paper, we shall use the following notation for these compact supports and finite index sets.

$$\operatorname{supp} \widehat{g} \subseteq I_{\boldsymbol{\Omega}_{\mathrm{c}}, \boldsymbol{\Omega}}, \qquad \boldsymbol{T}_{\boldsymbol{g}} \stackrel{\text{def}}{=} \tfrac{1}{\boldsymbol{\Omega}}, \qquad \boldsymbol{T}_{\boldsymbol{\gamma}} \stackrel{\text{def}}{=} \tfrac{1}{\boldsymbol{\Omega} + \boldsymbol{\omega}}, \tag{4.6a}$$

$$\operatorname{supp} S_H \subseteq I_{\boldsymbol{\omega}_{\mathrm{c}}, \boldsymbol{\omega}} \times I_{\boldsymbol{C}, \boldsymbol{L}}, \qquad \operatorname{supp} \widehat{H g} \subseteq \operatorname{supp} \widehat{\gamma} \subseteq I_{\boldsymbol{\Omega}_{\mathbf{c}} + \boldsymbol{\omega}_{\mathrm{c}}, \boldsymbol{\Omega} + \boldsymbol{\omega}}, \tag{4.6b}$$

$$\mathcal{K}, \mathcal{M} \subset \mathbb{Z}^d, \qquad |\mathcal{K}| < \infty, \qquad |\mathcal{M}| < \infty \qquad \text{and} \tag{4.6c}$$

$$g(\boldsymbol{m}\boldsymbol{T}_{\boldsymbol{g}}) = \gamma(\boldsymbol{k}\boldsymbol{T}_{\boldsymbol{\gamma}}) = (Hg)(\boldsymbol{k}\boldsymbol{T}_{\boldsymbol{\gamma}}) = 0 \quad \text{for} \quad \boldsymbol{k} \in \mathbb{Z}^d \setminus \mathcal{K} \text{ and } \boldsymbol{m} \in \mathbb{Z}^d \setminus \mathcal{M}. \tag{4.6d}$$

The corresponding supports and index sets for $g_{\boldsymbol{q},\boldsymbol{r}}$, $H g_{\boldsymbol{q},\boldsymbol{r}}$ and $\gamma_{\boldsymbol{q},\boldsymbol{r}}$ are easily computed from (4.5) above.

4.3 Computing the channel matrix

For spreading functions and window functions having the properties, supports and index sets given in (4.6) and Figure 3 (b), the following proposition provides us with a finite sum formula for computing the matrix elements $\langle H g_{\boldsymbol{q},\boldsymbol{r}}, \gamma_{\boldsymbol{q}',\boldsymbol{r}'} \rangle$ from samples of $H g_{\boldsymbol{q},\boldsymbol{r}}$ and $\gamma_{\boldsymbol{q}',\boldsymbol{r}'}$:

Proposition 2. *Let $u, v \in L^2(\mathbb{R}^d)$ be functions with compact, overlapping frequency supports satisfying*

$$\operatorname{supp} \widehat{u} \subseteq I_{\boldsymbol{C_u},\boldsymbol{B}}, \quad \operatorname{supp} \widehat{v} \subseteq I_{\boldsymbol{C_v},\boldsymbol{B}} \quad \text{and} \quad I_{\boldsymbol{C_{uv}},\boldsymbol{B_{uv}}} \stackrel{\text{def}}{=} I_{\boldsymbol{C_u},\boldsymbol{B}} \cap I_{\boldsymbol{C_v},\boldsymbol{B}} \neq \emptyset.$$

For $\boldsymbol{T} = \frac{1}{\boldsymbol{B}}$ and $\boldsymbol{k} \in \mathbb{Z}^d$, suppose that $u(\boldsymbol{kT}) \neq 0$ and $v(\boldsymbol{kT}) \neq 0$ only for $\boldsymbol{k}$ in some finite index sets $\mathcal{I}_u$ and $\mathcal{I}_v$, respectively. Denote with v_{bpf} the inverse Fourier transform of the restriction (bandpass filtering) of $\widehat{v}$ to the support of $\widehat{u}$, that is,

$$\widehat{v_{\text{bpf}}}(\boldsymbol{\xi}) \stackrel{\text{def}}{=} \widehat{v}(\boldsymbol{\xi}) \chi_{I_{\boldsymbol{C_{uv}},\boldsymbol{B_{uv}}}}(\boldsymbol{\xi}).$$

Then

$$\langle u, v \rangle_{L^2(\mathbb{R}^d)} = |\boldsymbol{T}| \sum_{\boldsymbol{k} \in \mathcal{I}_u} u(\boldsymbol{kT}) \overline{v_{\text{bpf}}(\boldsymbol{kT})}. \tag{4.7a}$$

Further, $v_{\text{bpf}} = v$ if $\boldsymbol{C_u} = \boldsymbol{C_v}$ and, otherwise,

$$v_{\text{bpf}}(\boldsymbol{kT}) = |\boldsymbol{T}| \sum_{\boldsymbol{k'} \in \mathcal{I}_v} v(\boldsymbol{k'T}) \mathrm{e}^{\mathrm{i}2\pi \langle \boldsymbol{C_{uv}}, (\boldsymbol{k}-\boldsymbol{k'})\boldsymbol{T} \rangle} \operatorname{sinc}_{\boldsymbol{B_{uv}}}((\boldsymbol{k}-\boldsymbol{k'})\boldsymbol{T}). \tag{4.7b}$$

Proof. (4.7a) follows from the Plancherel theorem and Parseval's identity:

$$\langle u, v \rangle_{L^2(\mathbb{R}^d)} = \langle \widehat{u}, \widehat{v} \rangle_{L^2(\mathbb{R}^d)} = \langle \widehat{u}, \widehat{v_{\text{bpf}}} \rangle_{L^2(I_{\boldsymbol{C_v},\boldsymbol{B}})} = |\boldsymbol{T}| \sum_{\boldsymbol{k} \in \mathcal{I}_u} u(\boldsymbol{kT}) \overline{v_{\text{bpf}}(\boldsymbol{kT})}.$$

Moreover, the sampling theorem (4.4a) and (2.1) implies that

$$\begin{aligned} v_{\text{bpf}}(\boldsymbol{kT}) &= \int_{\mathbb{R}^d} \widehat{v}(\boldsymbol{\xi}) \chi_{I_{\boldsymbol{C_{uv}},\boldsymbol{B_{uv}}}}(\boldsymbol{\xi}) \mathrm{e}^{\mathrm{i}2\pi \langle \boldsymbol{\xi}, \boldsymbol{kT} \rangle} \, \mathrm{d}\boldsymbol{\xi} \\ &= |\boldsymbol{T}| \sum_{\boldsymbol{k'} \in \mathcal{I}_v} v(\boldsymbol{k'T}) \int_{I_{\boldsymbol{C_{uv}},\boldsymbol{B_{uv}}}} \mathrm{e}^{\mathrm{i}2\pi \langle \boldsymbol{\xi}, (\boldsymbol{k}-\boldsymbol{k'})\boldsymbol{T} \rangle} \, \mathrm{d}\boldsymbol{\xi} \\ &= |\boldsymbol{T}| \sum_{\boldsymbol{k'} \in \mathcal{I}_v} v(\boldsymbol{k'T}) \mathrm{e}^{\mathrm{i}2\pi \langle \boldsymbol{C_{uv}}, (\boldsymbol{k}-\boldsymbol{k'})\boldsymbol{T} \rangle} \operatorname{sinc}_{\boldsymbol{B_{uv}}}((\boldsymbol{k}-\boldsymbol{k'})\boldsymbol{T}). \end{aligned}$$

□

Using (4.6) and (4.7a), we get, for example, that

$$\langle Hg, \gamma \rangle_{L^2(\mathbb{R}^d)} = |\boldsymbol{T_\gamma}| \sum_{\boldsymbol{k} \in \mathcal{K}} (Hg)(\boldsymbol{kT_\gamma}) \overline{\gamma(\boldsymbol{kT_\gamma})}$$

and it remains only to derive efficient formulas for the computation of the samples $(Hg)(\boldsymbol{kT_\gamma})$. For this, we derive the finite sum formula (4.10) below with nonzero terms only for $\boldsymbol{m} \in \mathcal{M}$ when $f = g$ (and similarly for $f = g_{\boldsymbol{q},\boldsymbol{r}}$)[4]. It is clear that the following proof holds for arbitrary samples $Hf(\boldsymbol{t_0})$, but by setting $\boldsymbol{t_0} = \boldsymbol{kT_\gamma}$ we get our results in exactly the form that we use later on.

[4]In (4.10) it is necessary for f to provide the finite summation index, since there can be a finite number of nonzero $S_H^{\boldsymbol{C_f},\Omega}(\cdot, \boldsymbol{kT_\gamma} - \boldsymbol{mT_g})$ and $(Hf)(\boldsymbol{kT_\gamma})$ (without alias effects due to undersampling) only if $\frac{\boldsymbol{T_\gamma}}{\boldsymbol{T_g}} \in \mathbb{Z}^d$ and $\boldsymbol{T_\gamma} = \frac{\boldsymbol{1}}{\boldsymbol{\Omega}+\boldsymbol{\omega}}$, that is, only if $\boldsymbol{\omega} = \boldsymbol{0}$.

Proposition 3. *Suppose that* $\boldsymbol{C_f}, \boldsymbol{\Omega} \in \mathbb{R}^d$, $f \in L^2(\mathbb{R}^d)$, $\operatorname{supp} \widehat{f} \subseteq I_{\boldsymbol{C_f},\boldsymbol{\Omega}}$ *and*

$$(f(\boldsymbol{m}\boldsymbol{T_f}))_{\boldsymbol{m}\in\mathbb{Z}^d} \in l^1(\mathbb{Z}^d), \qquad \text{with} \qquad \boldsymbol{T_f} \stackrel{\text{def}}{=} \frac{\boldsymbol{1}}{\boldsymbol{\Omega}}. \tag{4.8}$$

Let H *be a Hilbert–Schmidt operator with spreading function*

$$S_H \in C^\infty \cap L^2(\mathbb{R}^d) \quad \text{and} \quad \operatorname{supp} S_H \subseteq I_{\boldsymbol{\omega}_c,\boldsymbol{\omega}} \times I_{\boldsymbol{C},\boldsymbol{L}}. \tag{4.9a}$$

Define $S_H^{\boldsymbol{C_f},\boldsymbol{\Omega}}$ *to be the convolution*

$$S_H^{\boldsymbol{C_f},\boldsymbol{\Omega}}(\boldsymbol{\nu},\boldsymbol{t_0}) \stackrel{\text{def}}{=} \left(S_H(\boldsymbol{\nu},\cdot) * (\mathrm{e}^{\mathrm{i}2\pi\langle \boldsymbol{C_f}+\boldsymbol{\nu},\cdot\rangle} \operatorname{sinc}_{\boldsymbol{\Omega}}(\cdot))\right)(\boldsymbol{t_0}). \tag{4.9b}$$

Then for all $\boldsymbol{k} \in \mathbb{Z}^d$ *and* $\boldsymbol{T_\gamma} \in \mathbb{R}_+^d$, *we have*

$$(Hf)(\boldsymbol{k}\boldsymbol{T_\gamma}) = |\boldsymbol{T_f}| \sum_{\boldsymbol{m}\in\mathbb{Z}^d} f(\boldsymbol{m}\boldsymbol{T_f}) \left(S_H^{\boldsymbol{C_f},\boldsymbol{\Omega}}(\cdot, \boldsymbol{k}\boldsymbol{T_\gamma} - \boldsymbol{m}\boldsymbol{T_f})\right)\widehat{\ }(-\boldsymbol{m}\boldsymbol{T_f}). \tag{4.10}$$

Proof. From (2.9b) and the Fubini–Tonelli theorem,

$$\begin{aligned}(Hf)(\boldsymbol{t_0}) &= \int_{\mathbb{R}^d}\int_{\mathbb{R}^d} S_H(\boldsymbol{\nu},\boldsymbol{t}) f(\boldsymbol{t_0}-\boldsymbol{t}) \mathrm{e}^{\mathrm{i}2\pi\langle\boldsymbol{\nu},\boldsymbol{t_0}-\boldsymbol{t}\rangle}\,\mathrm{d}\boldsymbol{t}\,\mathrm{d}\boldsymbol{\nu} \\ &= \int_{\mathbb{R}^d} \left(S_H(\boldsymbol{\nu},\cdot) * (f(\cdot)\mathrm{e}^{\mathrm{i}2\pi\langle\boldsymbol{\nu},\cdot\rangle})\right)(\boldsymbol{t_0})\,\mathrm{d}\boldsymbol{\nu} \stackrel{\text{def}}{=} \int_{\mathbb{R}^d} f_{\boldsymbol{\nu}}(\boldsymbol{t_0})\,\mathrm{d}\boldsymbol{\nu},\end{aligned} \tag{4.11}$$

where the Nyquist sampling theorem (4.4b) and then (2.1) gives that

$$\begin{aligned}f_{\boldsymbol{\nu}}(\boldsymbol{t_0}) &= |\boldsymbol{T_f}| \sum_{\boldsymbol{m}\in\mathbb{Z}^d} f(\boldsymbol{m}\boldsymbol{T_f}) \left(S_H(\boldsymbol{\nu},\cdot) * (\mathrm{e}^{\mathrm{i}2\pi\langle \boldsymbol{C_f},\cdot-\boldsymbol{m}\boldsymbol{T_f}\rangle} \operatorname{sinc}_{\boldsymbol{\Omega}}(\cdot - \boldsymbol{m}\boldsymbol{T_f})\mathrm{e}^{\mathrm{i}2\pi\langle\boldsymbol{\nu},\cdot\rangle})\right)(\boldsymbol{t_0}) \\ &= |\boldsymbol{T_f}| \sum_{\boldsymbol{m}\in\mathbb{Z}^d} f(\boldsymbol{m}\boldsymbol{T_f}) \mathrm{e}^{\mathrm{i}2\pi\langle\boldsymbol{\nu},\boldsymbol{m}\boldsymbol{T_f}\rangle} \left(S_H(\boldsymbol{\nu},\cdot) * (\mathrm{e}^{\mathrm{i}2\pi\langle \boldsymbol{C_f}+\boldsymbol{\nu},\cdot\rangle} \operatorname{sinc}_{\boldsymbol{\Omega}}(\cdot))\right)(\boldsymbol{t_0} - \boldsymbol{m}\boldsymbol{T_f}).\end{aligned}$$

Insertion of this in (4.11) gives

$$(Hf)(\boldsymbol{k}\boldsymbol{T_\gamma}) = |\boldsymbol{T_f}| \int_{\mathbb{R}^d} \sum_{\boldsymbol{m}\in\mathbb{Z}^d} f(\boldsymbol{m}\boldsymbol{T_f}) \mathrm{e}^{\mathrm{i}2\pi\langle\boldsymbol{\nu},\boldsymbol{m}\boldsymbol{T_f}\rangle} S_H^{\boldsymbol{C_f},\boldsymbol{\Omega}}(\boldsymbol{\nu}, \boldsymbol{k}\boldsymbol{T_\gamma} - \boldsymbol{m}\boldsymbol{T_f})\,\mathrm{d}\boldsymbol{\nu}. \tag{4.12}$$

By (4.9a) and (4.9b), $S_H^{\boldsymbol{C_f},\boldsymbol{\Omega}}$ is bounded. Hence (4.8), (4.12) and the Fubini–Tonelli theorem provide

$$\begin{aligned}(Hf)(\boldsymbol{k}\boldsymbol{T_\gamma}) &= |\boldsymbol{T_f}| \sum_{\boldsymbol{m}\in\mathbb{Z}^d} f(\boldsymbol{m}\boldsymbol{T_f}) \int_{I_{\boldsymbol{\omega}_c,\boldsymbol{\omega}}} \mathrm{e}^{\mathrm{i}2\pi\langle\boldsymbol{\nu},\boldsymbol{m}\boldsymbol{T_f}\rangle} S_H^{\boldsymbol{C_f},\boldsymbol{\Omega}}(\boldsymbol{\nu}, \boldsymbol{k}\boldsymbol{T_\gamma} - \boldsymbol{m}\boldsymbol{T_f})\,\mathrm{d}\boldsymbol{\nu} \\ &= |\boldsymbol{T_f}| \sum_{\boldsymbol{m}\in\mathbb{Z}^d} f(\boldsymbol{m}\boldsymbol{T_f}) \left(S_H^{\boldsymbol{C_f},\boldsymbol{\Omega}}(\cdot, \boldsymbol{k}\boldsymbol{T_\gamma} - \boldsymbol{m}\boldsymbol{T_f})\right)\widehat{\ }(-\boldsymbol{m}\boldsymbol{T_f}),\end{aligned}$$

which proves (4.10) and concludes the proof. □

Next, we shall derive the finite sum formula (4.14) for computing the samples of $(S_H^{\boldsymbol{\Omega_c}+\boldsymbol{qb\Omega},\boldsymbol{\Omega}}(\cdot,\boldsymbol{t}))\widehat{\ }$ that are needed in (4.10) to compute $(Hg_{\boldsymbol{q},\boldsymbol{r}})(\boldsymbol{kT_\gamma})$ for a Gabor system

$$g_{\boldsymbol{q},\boldsymbol{r}} \stackrel{\text{def}}{=} T_{\boldsymbol{raT_g}} M_{\boldsymbol{qb\Omega}}\, g, \qquad (\boldsymbol{q},\boldsymbol{r}) \in \mathcal{Q}\times\mathcal{R}$$

for a finite index set $\mathcal{Q}\times\mathcal{R}\subseteq\mathbb{Z}^{2d}$. Equations (4.9b), (4.6a) and (4.6b) imply that $S_H^{\boldsymbol{\Omega_c}+\boldsymbol{qb\Omega},\boldsymbol{\Omega}}(\boldsymbol{\nu},\cdot)$ is obtained from bandpass filtering $S_H(\boldsymbol{\nu},\cdot)$ to the frequency band

$$\operatorname{supp}\widehat{g_{\boldsymbol{q},\boldsymbol{r}}}(\cdot-\boldsymbol{\nu}) = I_{\boldsymbol{\Omega_c}+\boldsymbol{qb\Omega}+\boldsymbol{\nu},\boldsymbol{\Omega}}, \qquad \text{where} \qquad \boldsymbol{\nu}\in\operatorname{supp} S_H^{\boldsymbol{\Omega_c}+\boldsymbol{qb\Omega},\boldsymbol{\Omega}}(\cdot,\boldsymbol{t}) \subseteq I_{\boldsymbol{\omega_c},\boldsymbol{\omega}}.$$

Hence, we can compute all $S_H^{\boldsymbol{\Omega_c}+\boldsymbol{qb\Omega},\boldsymbol{\Omega}}$ from the restriction of $\widehat{S_H(\boldsymbol{\nu},\cdot)}$ to the smallest interval $I_{\boldsymbol{\Omega_c'},\boldsymbol{\Omega'}}$ containing the union of the supports of all $\widehat{g_{\boldsymbol{q},\boldsymbol{r}}}(\cdot-\boldsymbol{\nu})$ for all $\boldsymbol{\nu}\in I_{\boldsymbol{\omega_c},\boldsymbol{\omega}}$, as illustrated for $d=1$ in Figure 5. This means that if $\mathcal{Q}=[\boldsymbol{q_0},\boldsymbol{q_1}]\cap\mathbb{Z}^d$, then

$$\boldsymbol{\Omega_c'} \stackrel{\text{def}}{=} \boldsymbol{\Omega_c} + \frac{\boldsymbol{q_0}+\boldsymbol{q_1}}{2}\boldsymbol{b\Omega} + \boldsymbol{\omega_c} \qquad \text{and} \qquad \boldsymbol{\Omega'} \stackrel{\text{def}}{=} (\boldsymbol{q_1}-\boldsymbol{q_0})\boldsymbol{b\Omega} + \boldsymbol{\Omega} + \boldsymbol{\omega}. \tag{4.13a}$$

This observation allows for a two-step discretization based on the system function properties summarized in Figure 3 (b), namely:

First, recall from Figure 3 (b) that h has compact support which is contained in some "box" $I_{\boldsymbol{C_0},\boldsymbol{L_0}}\times I_{\boldsymbol{C},\boldsymbol{L}}$, where $I_{\boldsymbol{C},\boldsymbol{L}}$ contains the support of $S_H(\boldsymbol{\nu},\cdot)$ for all $\boldsymbol{\nu}$. Recall also that due to the smooth truncation in Section 3.3, $h(\cdot,\boldsymbol{t})$ is supported in an interval $I_{\boldsymbol{C_0},\boldsymbol{L_0}}$, which is large enough not to affect the channel output in the time interval under consideration. This together with the impulse response integral representation (2.9c) of H gives that $\operatorname{supp} h(\cdot,\boldsymbol{t})\subseteq I_{\boldsymbol{C_0},\boldsymbol{L_0}}$ must be large enough to contain the support of $Hg_{\boldsymbol{q},\boldsymbol{r}}$ for all $r\in\mathcal{R}$. Using element-wise addition of sets, this condition has the form

$$\operatorname{supp} g + \mathcal{R}\boldsymbol{aT_g} + I_{\boldsymbol{C},\boldsymbol{L}} \subseteq I_{\boldsymbol{C_0},\boldsymbol{L_0}}. \tag{4.13b}$$

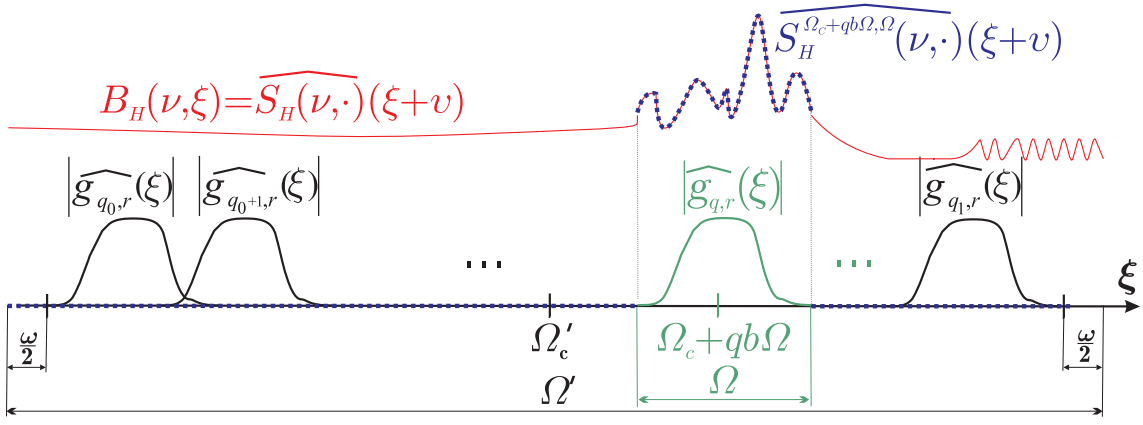

Figure 5: For Gabor frames $g_{\boldsymbol{q},\boldsymbol{r}} \stackrel{\text{def}}{=} T_{\boldsymbol{raT_g}} M_{\boldsymbol{qb\Omega}} g$ with $\boldsymbol{q}\in\mathcal{Q}\stackrel{\text{def}}{=}[\boldsymbol{q_0},\boldsymbol{q_1}]\cap\mathbb{Z}^d$, the function $|\widehat{g_{\boldsymbol{q},\boldsymbol{r}}}|$ depends only on $\boldsymbol{q}$. Proposition 3 shows how to compute all $Hg_{\boldsymbol{q},\boldsymbol{r}}$ only from the restriction of $\widehat{S_H(\boldsymbol{\nu},\cdot)}$ to any interval $I_{\boldsymbol{\Omega_c'},\boldsymbol{\Omega'}}$ containing the supports of all $\widehat{g_{\boldsymbol{q},\boldsymbol{r}}}(\cdot-\boldsymbol{\nu})$ for all $\boldsymbol{\nu}\in I_{\boldsymbol{\omega_c},\boldsymbol{\omega}}$, as is illustrated here for minimal Ω' and $d=1$.

It follows that

$$\operatorname{supp}\widehat{S_H(\cdot,\boldsymbol{t})}(\boldsymbol{t_0}) = \operatorname{supp} h(\boldsymbol{t}-\boldsymbol{t_0},\boldsymbol{t}) = \left\{(\boldsymbol{t_0},\boldsymbol{t}) \in \mathbb{R}^{2d} : \boldsymbol{t} \in I_{\boldsymbol{C},\boldsymbol{L}} \text{ and } \boldsymbol{t_0} \in I_{\boldsymbol{t}-\boldsymbol{C_0},\boldsymbol{L_0}}\right\}.$$

Due to this compact support set and the subexponential decay of $S_H(\cdot,\boldsymbol{t})$, we can apply and truncate the Nyquist sampling theorem (4.4b) to

$$\begin{aligned} S_H(\boldsymbol{\nu},\boldsymbol{t}) &= |\boldsymbol{\omega_0}| \sum_{\boldsymbol{n}\in\mathcal{N}} S_H(\boldsymbol{n\omega_0},\boldsymbol{t}) \mathrm{e}^{\mathrm{i}2\pi\langle \boldsymbol{t}-\boldsymbol{C_0},\boldsymbol{\nu}-\boldsymbol{n\omega_0}\rangle} \operatorname{sinc}_{\boldsymbol{L_0}}(\boldsymbol{\nu}-\boldsymbol{n\omega_0}), \\ |\mathcal{N}| &< \infty \qquad \text{and} \qquad \boldsymbol{\omega}_0 \stackrel{\text{def}}{=} \frac{1}{\boldsymbol{L_0}}. \end{aligned} \tag{4.13c}$$

Second, we shall use that only the restriction of $\widehat{S_H(\boldsymbol{\nu},\cdot)} = B_H(\boldsymbol{\nu},\cdot-\boldsymbol{\nu})$ to $I_{\boldsymbol{\Omega_c'},\boldsymbol{\Omega'}}$ is of importance for our computations. Since $S_H(\boldsymbol{\nu},\cdot)$ has compact support, we know from Section 2.2 that there is a smooth truncation of $\widehat{S_H(\boldsymbol{\nu},\cdot)}$ to a C^∞ function $\widehat{S^{\boldsymbol{\Omega''}}_{\boldsymbol{\Omega_c''}}(\boldsymbol{\nu},\cdot)}$ such that

$$\widehat{S^{\boldsymbol{\Omega''}}_{\boldsymbol{\Omega_c''}}(\boldsymbol{\nu},\boldsymbol{\cdot})} = \widehat{S_H(\boldsymbol{\nu},\boldsymbol{\cdot})} \text{ in } I_{\boldsymbol{\Omega_c'},\boldsymbol{\Omega'}}, \qquad \operatorname{supp}\widehat{S^{\boldsymbol{\Omega''}}_{\boldsymbol{\Omega_c''}}(\boldsymbol{\nu},\cdot)} \subseteq I_{\boldsymbol{\Omega_c''},\boldsymbol{\Omega''}} \tag{4.13d}$$

with $I_{\boldsymbol{\Omega_c''},\boldsymbol{\Omega''}}$ compact and such that

$$S^{\boldsymbol{\Omega''}}_{\boldsymbol{\Omega_c''}}(\boldsymbol{\nu},\cdot) \text{ decays subexponentially.} \tag{4.13e}$$

Hence we can apply the sampling theorem (4.4a) to $\widehat{S^{\boldsymbol{\Omega''}}_{\boldsymbol{\Omega_c''}}(\boldsymbol{\nu},\cdot)}$ and truncate it with no or negligible error to a finite sum

$$\begin{aligned} \widehat{S^{\boldsymbol{\Omega''}}_{\boldsymbol{\Omega_c''}}(\boldsymbol{\nu},\boldsymbol{\cdot})}(\boldsymbol{\xi}) &= |\boldsymbol{T''}|\, \chi_{I_{\boldsymbol{\Omega_c''},\boldsymbol{\Omega''}}}(\boldsymbol{\xi}) \sum_{\boldsymbol{p}\in\mathcal{P}} S^{\boldsymbol{\Omega''}}_{\boldsymbol{\Omega_c''}}(\boldsymbol{\nu},\boldsymbol{pT''}) \mathrm{e}^{-\mathrm{i}2\pi\langle\boldsymbol{\xi},\boldsymbol{pT''}\rangle}, \\ |\mathcal{P}| &< \infty \qquad \text{and} \qquad \boldsymbol{T''} \stackrel{\text{def}}{=} \frac{\mathbf{1}}{\boldsymbol{\Omega''}}. \end{aligned} \tag{4.13f}$$

We are now ready to state our final proposition.

Proposition 4. *For the functions and supports defined in* (4.6), (4.9b) *and* (4.13), *set* $\boldsymbol{\Omega_{c,q}} \stackrel{\text{def}}{=} \boldsymbol{\Omega_c} + \boldsymbol{qb\Omega}$ *for all* $\boldsymbol{q} \in \mathcal{Q}$. *Then*

$$\begin{aligned} \widehat{S_H^{\boldsymbol{\Omega_{c,q}},\boldsymbol{\Omega}}}(\cdot,\boldsymbol{t})(\boldsymbol{t_0}) = |\boldsymbol{\omega_0 T''}|\, \chi_{I_{\boldsymbol{C_0},\boldsymbol{L_0}}}(\boldsymbol{t}-\boldsymbol{t_0}) \sum_{\boldsymbol{p}\in\mathcal{P}} \mathrm{e}^{\mathrm{i}2\pi\langle\boldsymbol{\Omega_{c,q}},\boldsymbol{t}-\boldsymbol{pT''}\rangle} \operatorname{sinc}_{\boldsymbol{\Omega}}(\boldsymbol{t}-\boldsymbol{pT''}) \times \\ \times \sum_{\boldsymbol{n}\in\mathcal{N}} S^{\boldsymbol{\Omega''}}_{\boldsymbol{\Omega_c''}}(\boldsymbol{n\omega_0},\boldsymbol{pT''}) \mathrm{e}^{\mathrm{i}2\pi\langle\boldsymbol{t}-\boldsymbol{t_0}-\boldsymbol{pT''},\boldsymbol{n\omega_0}\rangle}. \end{aligned} \tag{4.14}$$

Proof. Note first that if $\boldsymbol{\xi} \in I_{\boldsymbol{\Omega_{c,q}}+\boldsymbol{\nu},\boldsymbol{\Omega}}$, then for all $\boldsymbol{n\omega_0} \in I_{\boldsymbol{\omega_c},\boldsymbol{\omega}}$,

$$\boldsymbol{\xi} - (\boldsymbol{\nu}-\boldsymbol{n\omega_0}) \in I_{\boldsymbol{\Omega_{c,q}}+\boldsymbol{n\omega_0},\boldsymbol{\Omega}} \subseteq I_{\boldsymbol{\Omega_c'},\boldsymbol{\Omega'}},$$

so that (4.13d) implies that

$$\widehat{S_H(\boldsymbol{\nu},\cdot)}(\boldsymbol{\xi}-(\boldsymbol{\nu}-\boldsymbol{n\omega_0}))\chi_{I_{\boldsymbol{\Omega_{c,q}}+\boldsymbol{\nu},\boldsymbol{\Omega}}}(\boldsymbol{\xi}) = \widehat{S^{\boldsymbol{\Omega''}}_{\boldsymbol{\Omega_c''}}(\boldsymbol{\nu},\cdot)}(\boldsymbol{\xi}-(\boldsymbol{\nu}-\boldsymbol{n\omega_0}))\chi_{I_{\boldsymbol{\Omega_{c,q}}+\boldsymbol{\nu},\boldsymbol{\Omega}}}(\boldsymbol{\xi}).$$

Hence, it follows from (4.13), the definition (4.9b) and (2.1) that for all $\boldsymbol{\nu} \in I_{\boldsymbol{\omega}_c,\boldsymbol{\omega}}$,

$$\widehat{S_H^{\boldsymbol{\Omega}_{c,q},\boldsymbol{\Omega}}(\boldsymbol{\nu},\cdot)}(\boldsymbol{\xi}) = \widehat{S_H(\boldsymbol{\nu},\cdot)}(\boldsymbol{\xi})\chi_{I_{\boldsymbol{\Omega}_{c,q}+\boldsymbol{\nu},\boldsymbol{\Omega}}}(\boldsymbol{\xi})$$

$$= |\boldsymbol{\omega_0}| \sum_{\boldsymbol{n}\in\mathcal{N}} \widehat{S_H(\boldsymbol{n\omega_0},\cdot)}(\boldsymbol{\xi}-(\boldsymbol{\nu}-\boldsymbol{n\omega_0}))\chi_{I_{\boldsymbol{\Omega}_{c,q}+\boldsymbol{\nu},\boldsymbol{\Omega}}}(\boldsymbol{\xi})\mathrm{e}^{-\mathrm{i}2\pi\langle \boldsymbol{C_0},\boldsymbol{\nu}-\boldsymbol{n\omega_0}\rangle}\operatorname{sinc}_{\boldsymbol{L_0}}(\boldsymbol{\nu}-\boldsymbol{n\omega_0}) =$$
$$= |\boldsymbol{\omega_0 T''}| \sum_{\boldsymbol{n}\in\mathcal{N}}\sum_{\boldsymbol{p}\in\mathcal{P}} S_{\boldsymbol{\Omega_c''}}^{\boldsymbol{\Omega''}}(\boldsymbol{n\omega_0},\boldsymbol{pT''})\mathrm{e}^{-\mathrm{i}2\pi\langle \boldsymbol{\xi}-(\boldsymbol{\nu}-\boldsymbol{n\omega_0}),\boldsymbol{pT''}\rangle}\chi_{I_{\boldsymbol{\Omega}_{c,q}+\boldsymbol{\nu},\boldsymbol{\Omega}}}(\boldsymbol{\xi})\times$$
$$\times\, \mathrm{e}^{-\mathrm{i}2\pi\langle \boldsymbol{C_0},\boldsymbol{\nu}-\boldsymbol{n\omega_0}\rangle}\operatorname{sinc}_{\boldsymbol{L_0}}(\boldsymbol{\nu}-\boldsymbol{n\omega_0})$$

Inverse Fourier transformation and (2.1) again gives

$$S_H^{\boldsymbol{\Omega}_{c,q},\boldsymbol{\Omega}}(\boldsymbol{\nu},\boldsymbol{t}) = |\boldsymbol{\omega_0 T''}| \sum_{\boldsymbol{n}\in\mathcal{N}}\sum_{\boldsymbol{p}\in\mathcal{P}} S_{\boldsymbol{\Omega_c''}}^{\boldsymbol{\Omega''}}(\boldsymbol{n\omega_0},\boldsymbol{pT''}) \int_{I_{\boldsymbol{\Omega}_{c,q}+\boldsymbol{\nu},\boldsymbol{\Omega}}} \mathrm{e}^{\mathrm{i}2\pi\langle \boldsymbol{\xi},\boldsymbol{t}-\boldsymbol{pT''}\rangle}\,\mathrm{d}\boldsymbol{\xi}\times$$
$$\times\, \mathrm{e}^{\mathrm{i}2\pi\langle \boldsymbol{pT''}-\boldsymbol{C_0},\boldsymbol{\nu}-\boldsymbol{n\omega_0}\rangle}\operatorname{sinc}_{\boldsymbol{L_0}}(\boldsymbol{\nu}-\boldsymbol{n\omega_0})$$
$$= |\boldsymbol{\omega_0 T''}| \sum_{\boldsymbol{n}\in\mathcal{N}}\sum_{\boldsymbol{p}\in\mathcal{P}} S_{\boldsymbol{\Omega_c''}}^{\boldsymbol{\Omega''}}(\boldsymbol{n\omega_0},\boldsymbol{pT''})\mathrm{e}^{\mathrm{i}2\pi\langle \boldsymbol{\Omega}_{c,q}+\boldsymbol{\nu},\boldsymbol{t}-\boldsymbol{pT''}\rangle}\times$$
$$\times\, \operatorname{sinc}_{\boldsymbol{\Omega}}(\boldsymbol{t}-\boldsymbol{pT''})\mathrm{e}^{-\mathrm{i}2\pi\langle \boldsymbol{pT''}-\boldsymbol{C_0},\boldsymbol{n\omega_0}\rangle}\mathrm{e}^{\mathrm{i}2\pi\langle \boldsymbol{pT''}-\boldsymbol{C_0},\boldsymbol{\nu}\rangle}\operatorname{sinc}_{\boldsymbol{L_0}}(\boldsymbol{\nu}-\boldsymbol{n\omega_0}).$$

Since $\operatorname{sinc}_{\boldsymbol{L_0}}(\cdot-\boldsymbol{n\omega_0})$ is the inverse Fourier transform of $\chi_{I_{\boldsymbol{0},\boldsymbol{L_0}}}(\cdot)\mathrm{e}^{-\mathrm{i}2\pi\langle\cdot,\boldsymbol{n\omega_0}\rangle}$,

$$\widehat{S_H^{\boldsymbol{\Omega}_{c,q},\boldsymbol{\Omega}}(\cdot,\boldsymbol{t})}(\boldsymbol{t_0})$$
$$= |\boldsymbol{\omega_0 T''}| \sum_{\boldsymbol{n}\in\mathcal{N}}\sum_{\boldsymbol{p}\in\mathcal{P}} S_{\boldsymbol{\Omega_c''}}^{\boldsymbol{\Omega''}}(\boldsymbol{n\omega_0},\boldsymbol{pT''})\mathrm{e}^{\mathrm{i}2\pi\langle \boldsymbol{\Omega}_{c,q},\boldsymbol{t}-\boldsymbol{pT''}\rangle}\operatorname{sinc}_{\boldsymbol{\Omega}}(\boldsymbol{t}-\boldsymbol{pT''})\times$$
$$\times \int_{\mathbb{R}^d} \mathrm{e}^{-\mathrm{i}2\pi\langle \boldsymbol{\nu},\boldsymbol{t_0}+\boldsymbol{C_0}-\boldsymbol{t}\rangle}\operatorname{sinc}_{\boldsymbol{L_0}}(\boldsymbol{\nu}-\boldsymbol{n\omega_0})\,\mathrm{d}\boldsymbol{\nu}\mathrm{e}^{-\mathrm{i}2\pi\langle \boldsymbol{pT''}-\boldsymbol{C_0},\boldsymbol{n\omega_0}\rangle}$$
$$= |\boldsymbol{\omega_0 T''}| \sum_{\boldsymbol{n}\in\mathcal{N}}\sum_{\boldsymbol{p}\in\mathcal{P}} S_{\boldsymbol{\Omega_c''}}^{\boldsymbol{\Omega''}}(\boldsymbol{n\omega_0},\boldsymbol{pT''})\mathrm{e}^{\mathrm{i}2\pi\langle \boldsymbol{\Omega}_{c,q},\boldsymbol{t}-\boldsymbol{pT''}\rangle}\operatorname{sinc}_{\boldsymbol{\Omega}}(\boldsymbol{t}-\boldsymbol{pT''})\mathrm{e}^{-\mathrm{i}2\pi\langle \boldsymbol{pT''}-\boldsymbol{C_0},\boldsymbol{n\omega_0}\rangle}\times$$
$$\times\, \chi_{I_{\boldsymbol{0},\boldsymbol{L_0}}}(\boldsymbol{t_0}+\boldsymbol{C_0}-\boldsymbol{t})\mathrm{e}^{-\mathrm{i}2\pi\langle \boldsymbol{t_0}+\boldsymbol{C_0}-\boldsymbol{t},\boldsymbol{n\omega_0}\rangle}.$$

This proves (4.14). □

Remark. For physical wireless communications channels, we deduced a spreading function integral representation (3.9c) of the channel which is valid for functions with frequency localization "near ξ_0". For the OFDM and Satellite communications examples in Section 6, this assumption holds for the entire frequency band $I_{\Omega_c',\Omega'}$, since Ω'/Ω_c' is of the size $3\cdot 10^{-3}$ and $2\cdot 10^{-3}$, respectively. Then, the coefficients $S_{\boldsymbol{\Omega_c''}}^{\boldsymbol{\Omega''}}(\boldsymbol{n\omega_0},\boldsymbol{pT''})$ above characterize the channel throughout this frequency band. In the Underwater communications example, however, this is not the case, but the above theory can still be applied to each computed $Hg_{\boldsymbol{q},\boldsymbol{r}}$ as long as the relative bandwidth Ω of $g_{q,r}$ is much smaller than the carrier frequency $\Omega_{c,q} \stackrel{\text{def}}{=} \Omega_c + qb\Omega$.

Normally we also want Ω to be larger than the maximum Doppler shift $|\nu_{\mathrm{P}}\xi| = \left|\frac{V_{\mathrm{P}}}{V_{\mathrm{w}}}\xi\right|$ of (3.2), so as a rule of thumb $|V_{\mathrm{P}}/V_{\mathrm{w}}|$ should be very small, so that a larger but still small Ω/ξ can be chosen. In this case, and provided that the attenuation factor $A_\xi(\mathrm{P})$ in (3.3) is slowly varying with ξ, the following modifications allow for a "wideband use" of the propositions in this section:

1. Equation (3.9c) splits into separate operators H_q for basis functions $g_{q,r}$ with center frequency $\Omega_{\mathrm{c},q}$. For some compact sets $K_q \subseteq (-\Omega_{\mathrm{c},q}, \Omega_{\mathrm{c},q})$, these operators have integral representation

$$H_q g_{q,r}(\cdot) = \int_{K_q\times[A,\infty)} S_{H_q}(\nu',t)(T_t M_{\nu'} g_{q,r})(\cdot)\,\mathrm{d}(\nu',t),$$
$$S_{H_q}(\nu',t) \stackrel{\mathrm{def}}{=} \frac{1}{\Omega_{\mathbf{c},q}} r_{\xi_0}\left(\frac{\nu'}{\Omega_{\mathbf{c},q}},t\right)\mathrm{e}^{-\alpha_{\xi_0}t}\chi_{K\times[A,\infty)}\left(\frac{\nu'}{\Omega_{\mathbf{c},q}},t\right).$$

2. A straightforward multivariate extension of (3.9c) gives an operator spreading function S_H for signals with frequency localization near some fixed center frequency $\boldsymbol{\xi_0}$. Then the operator's action on narrowband functions $g_{\boldsymbol{q},\boldsymbol{r}}$ with center frequency $\boldsymbol{\Omega_{\mathbf{c},q}} \stackrel{\mathrm{def}}{=} \boldsymbol{\Omega_{\mathbf{c}}} + \boldsymbol{qb\Omega}$ is given by a spreading function

$$S_{H_{\boldsymbol{q}}}(\boldsymbol{\nu},\boldsymbol{t}) \stackrel{\mathrm{def}}{=} \left|\frac{\boldsymbol{\xi_0}}{\boldsymbol{\Omega_{\mathbf{c},q}}}\right| S_H\left(\frac{\boldsymbol{\xi_0}}{\boldsymbol{\Omega_{\mathbf{c},q}}}\boldsymbol{\nu},\boldsymbol{t}\right) \tag{4.15}$$

3. With $\boldsymbol{\xi_0}$ chosen so that all $[\mathbf{0},\boldsymbol{\Omega_{\mathbf{c},q}}] \subseteq [\mathbf{0},\boldsymbol{\xi_0}]$, we keep the notation (4.6), now with $I_{\boldsymbol{\omega}_{\mathrm{c}},\boldsymbol{\omega}} \times I_{\boldsymbol{C},\boldsymbol{L}}$ being the smallest interval containing $\operatorname{supp} S_{H_{\boldsymbol{q}}}$ for all $\boldsymbol{q} \in \mathcal{Q}$.

4. These changes do not affect Propositions 1–3, but if $\widehat{S_H(\cdot,\boldsymbol{t})}$ has the support given by (4.13b), then the dilation with a factor $\frac{\boldsymbol{\xi_0}}{\boldsymbol{\Omega_{\mathbf{c},q}}}$ in (5) gives that $\widehat{S_{H_{\boldsymbol{q}}}(\cdot,\boldsymbol{t})}$ has its support in

$$I_{\boldsymbol{C_{0,q}},\boldsymbol{L_{0,q}}} \stackrel{\mathrm{def}}{=} I_{\frac{\boldsymbol{\xi_0}}{\boldsymbol{\Omega_{\mathbf{c},q}}}\boldsymbol{C_0},\frac{\boldsymbol{\xi_0}}{\boldsymbol{\Omega_{\mathbf{c},q}}}\boldsymbol{L_0}}.$$

5. Hence we also know from (4.15) that if $\boldsymbol{\omega_{0,q}} \stackrel{\mathrm{def}}{=} \frac{1}{\boldsymbol{L_{0,q}}}$, then

$$|\boldsymbol{\omega_{0,q}}|\, S_{H_{\boldsymbol{q}}}(\boldsymbol{n\omega_{0,q}},\boldsymbol{t}) = \left|\frac{\boldsymbol{\xi_0}}{\boldsymbol{\Omega_{\mathbf{c},q}}}\boldsymbol{\omega_{0,q}}\right| S_H\left(\boldsymbol{n}\frac{\boldsymbol{\xi_0}}{\boldsymbol{\Omega_{\mathbf{c},q}}}\boldsymbol{\omega_{0,q}},\boldsymbol{t}\right) \stackrel{\mathrm{def}}{=} |\boldsymbol{\omega_0}|\, S_H\left(\boldsymbol{n\omega_0},\boldsymbol{t}\right)$$

so that (4.13c) takes the form

$$S_{H_{\boldsymbol{q}}}(\boldsymbol{\nu},\boldsymbol{t}) = |\boldsymbol{\omega_0}| \sum_{\boldsymbol{n}\in\mathcal{N}} S_H(\boldsymbol{n\omega_0},\boldsymbol{t})\mathrm{e}^{\mathrm{i}2\pi\langle \boldsymbol{t}-\boldsymbol{C_{0,q}},\boldsymbol{\nu}-\boldsymbol{n\omega_{0,q}}\rangle}\operatorname{sinc}_{\boldsymbol{L_{0,q}}}(\boldsymbol{\nu}-\boldsymbol{n\omega_{0,q}}).$$

Insertion of this in the proof of Proposition 4 then changes (4.14) into the following formula for computing all $\widehat{S_{H_{\boldsymbol{q}}}^{\boldsymbol{\Omega_{\mathbf{c},q}},\boldsymbol{\Omega}}(\cdot,\boldsymbol{t})}$ from the same coefficients $S_{\boldsymbol{\Omega_{\mathbf{c}}''}}^{\boldsymbol{\Omega''}}(\boldsymbol{n\omega_0},\boldsymbol{pT''})$:

$$\widehat{S_{H_{\boldsymbol{q}}}^{\boldsymbol{\Omega_{\mathbf{c},q}},\boldsymbol{\Omega}}(\cdot,\boldsymbol{t})}(\boldsymbol{t_0}) = |\boldsymbol{\omega_0 T''}|\,\chi_{\boldsymbol{C_{0,q}},\boldsymbol{L_{0,q}}}(\boldsymbol{t}-\boldsymbol{t_0})\sum_{\boldsymbol{p}\in\mathcal{P}}\mathrm{e}^{\mathrm{i}2\pi\langle\boldsymbol{\Omega_{\mathbf{c},q}},\boldsymbol{t}-\boldsymbol{pT''}\rangle}\operatorname{sinc}_{\boldsymbol{\Omega}}(\boldsymbol{t}-\boldsymbol{pT''})\times$$
$$\times\sum_{\boldsymbol{n}\in\mathcal{N}} S_{\boldsymbol{\Omega_{\mathbf{c}}''}}^{\boldsymbol{\Omega''}}(\boldsymbol{n\omega_0},\boldsymbol{pT''})\mathrm{e}^{\mathrm{i}2\pi\langle\boldsymbol{t}-\boldsymbol{t_0}-\boldsymbol{pT''},\boldsymbol{n\omega_{0,q}}\rangle}. \tag{4.16}$$

REMARK. The described procedure can also be used for the analysis of channel operators applied to signals not generated by a Gabor frame with narrowband window function, as well as for the analysis of Hilbert–Schmidt operators satisfying the properties in Figure 3 (b) in general. Then, the narrowband windows g and γ are chosen to investigate properties of the operator. Diagonalizati0n properties are still useful, but now in the sense that they give a "simple" discretized descriptions of the operator.

REMARK. The derivation of equation (4.2) does not require $(g_{\boldsymbol{q},\boldsymbol{r}})$ or $(\gamma_{\boldsymbol{q}',\boldsymbol{r}'})$ to be *Gabor* frames. Thus one possible future variation of the results of this paper is to use, for example, compactly supported wavelet bases, such as B-spline, Daubechies or Morlet wavelets, which also give synthesis and analysis of signals that can be reconstructed from a finite number of sample values with bandlimiting conditions replaced by projections on certain shift-invariant wavelet subspaces [EG05, EG04].

Gabor bases are a natural first choice for the OFDM applications that we have described. Wavelet frame modifications of our algorithm might be more interesting for a wideband communications scenario since the "frequency-dependent modulation" in (3.2a) is actually a dilation that can only be reduced to a modulation in the narrowband scenario described in Section 3.2.

5 The algorithm and its implementation

In Section 5.1 we summarize the results of the last section in an algorithm for the coefficient operator matrix computation. Then we propose some further refinements for a fast implementation and compute its complexity in Section 5.2, followed by suggestions for how to choose windows and parameters in Section 5.3.

5.1 The algorithm

The results of Section 4 lead to the following procedure for computing the coefficient operator matrix of a Hilbert-Schmidt operator satisfying the conditions outlined in Figure 3(b).

1. Choose the spreading function coefficients $S_{\Omega_c''}^{\Omega''}(\boldsymbol{n\omega_0}, \boldsymbol{pT''})$, the Gabor windows g, γ and set all parameters to values typical for the application at hand. We give suggestions for how to do this in Section 5.3 and 6.

2. For all $\boldsymbol{q}, \boldsymbol{q'} \in \mathcal{Q}$ and $\boldsymbol{r}, \boldsymbol{r'} \in \mathcal{R}$, compute the matrix element $\langle Hg_{\boldsymbol{q},\boldsymbol{r}}, \gamma_{\boldsymbol{q}',\boldsymbol{r}'}\rangle$ in the following way:

   (a) Compute the samples, index sets and supports of $g_{\boldsymbol{q},\boldsymbol{r}}$ and $\gamma_{\boldsymbol{q}',\boldsymbol{r}'}$ as described in (4.5) and (4.6).

   (b) Compute the matrix elements $\langle Hg_{\boldsymbol{q},\boldsymbol{r}}, \gamma_{\boldsymbol{q}',\boldsymbol{r}'}\rangle$ by applying (4.7) to $Hg_{\boldsymbol{q},\boldsymbol{r}}$ and $\gamma_{\boldsymbol{q}',\boldsymbol{r}'}$. For this we need the samples $(Hg_{\boldsymbol{q},\boldsymbol{r}})(\boldsymbol{kT_\gamma})$, which we obtain by setting $f = g_{\boldsymbol{q},\boldsymbol{r}}$ in the finite sum formula (4.10), in which we get the samples

$$\left(S_H^{\boldsymbol{\Omega_c}+\boldsymbol{Q}\flat\boldsymbol{\Omega},\boldsymbol{\Omega}}(\cdot, \boldsymbol{kT_\gamma} - \boldsymbol{mT_g})\right)\widehat{\ }(-\boldsymbol{mT_g})$$

from the finite sum formula (4.14) or (4.16) for the more wideband underwater communications example below.

See [GP05] for a fully documented MATLAB implementation of this procedure in the univariate case.

5.2 Refinements and complexity

For an efficient implementation, we also recommend the following two refinements of the above algorithm:

1. In step 2 (b), the sum (4.7b) can be obtained from a simple modulation of a small number of sample values which should be computed in advance.

   In fact, for the setup given in (4.6a) let $\mathcal{I}_{\boldsymbol{q}}$ and $\widehat{\mathcal{I}}_{\boldsymbol{r}}$ be the smallest intervals such that $Hg_{\boldsymbol{q},\boldsymbol{r}} \subseteq \mathcal{I}_{\boldsymbol{r}}$ and $\widehat{Hg_{\boldsymbol{q},\boldsymbol{r}}} \subseteq \widehat{\mathcal{I}}_{\boldsymbol{q}}$ for all $\boldsymbol{q} \in \mathcal{Q}$ and $\boldsymbol{r} \in \mathcal{R}$. We shall see below that there is only a small number of $\boldsymbol{q'} \in \mathcal{Q}$ and $\boldsymbol{r}, \boldsymbol{r'} \in \mathcal{R}$ such that the overlaps $\mathcal{I}_{\boldsymbol{r}} \cap \operatorname{supp} \gamma_{\boldsymbol{q'},\boldsymbol{r'}}$ and $\operatorname{supp} \widehat{\mathcal{I}}_{\boldsymbol{0}} \cap \operatorname{supp} \widehat{\gamma_{\boldsymbol{r'},\boldsymbol{q'}}}$ are nonempty. With (4.7b) computed for the above overlaps, we only need simple modulation to also compute (4.7b) for $u = Hg_{\boldsymbol{q},\boldsymbol{r}}$, $v = \gamma_{\boldsymbol{q'},\boldsymbol{r'}}$, $\boldsymbol{q}, \boldsymbol{q'} \in \mathcal{Q}$ and $\boldsymbol{r}, \boldsymbol{r'} \in \mathcal{R}$ in Proposition 2.

2. Recall from (4.14) and Figure 5 that $|\mathcal{N}| \cdot |\mathcal{P}|$ is the number of Fourier coefficients needed to describe the smooth truncation $S^{\boldsymbol{\Omega''}}_{\boldsymbol{\Omega''_c}}$ of $B_H(\boldsymbol{\nu}, \cdot)$ to the frequency interval $I_{\boldsymbol{\Omega''_c},\boldsymbol{\Omega''}}$.

   It is clear from Proposition 4 that $|\mathcal{P}|$ is proportional to the total bandwidth $I_{\boldsymbol{\Omega'_c},\boldsymbol{\Omega'}}$ occupied by the Gabor basis $(g_{\boldsymbol{q},\boldsymbol{r}})$ and thus also proportional to $|\mathcal{Q}|$. This dependence on $|\mathcal{Q}|$ comes from our choice to compute all $Hg_{\boldsymbol{q},\boldsymbol{r}}$ from the same $S^{\boldsymbol{\Omega''}}_{\boldsymbol{\Omega''_c}}$. This simplified the presentation and is also memory-efficient, since it minimizes the total bandwidth $I_{\boldsymbol{\Omega''_c},\boldsymbol{\Omega''}} \setminus I_{\boldsymbol{\Omega'_c},\boldsymbol{\Omega'}}$ added for the smooth truncation that is necessary to obtain a finite index set $\mathcal{P}$ finite. Thus it also minimizes the total number of coefficients that are needed to describe the channel behaviour in the entire frequency band $I_{\boldsymbol{\Omega'_c},\boldsymbol{\Omega'}}$. The resulting algorithm is also fast enough for the 2048×2048-matrix examples of Section 6.

   For more computational efficiency when $|\mathcal{Q}|$ is large, however, it is favourable to do a separate smooth cut-off $S^{\boldsymbol{\Omega''_q}}_{\boldsymbol{\Omega''_{c,q}}}$ of $B_H(\boldsymbol{\nu}, \cdot)$ for every $\boldsymbol{q}$ to an interval $I_{\boldsymbol{\Omega''_{c,q}},\boldsymbol{\Omega''_q}} \supseteq I_{\boldsymbol{\Omega_c}+\boldsymbol{q}b\boldsymbol{\Omega},\boldsymbol{\Omega}}$. This results in the coefficients $S^{\boldsymbol{\Omega''}}_{\boldsymbol{\Omega''_c}}(\boldsymbol{n\omega_0}, \boldsymbol{pT''})$ of (4.14) being replaced with a larger total number of coefficients, but with index sets $|\mathcal{P}_{\boldsymbol{q}}|$ proportional to $|\boldsymbol{\Omega}|$.

With these refinements, the complexity of the above procedure is that of one nested sum over the index sets $\mathcal{K}$, $\mathcal{M}$, $\mathcal{N}$ and $\mathcal{P}$ for each $\boldsymbol{q}, \boldsymbol{q'} \in \mathcal{Q}$ and $\boldsymbol{r}, \boldsymbol{r'} \in \mathcal{R}$. Altogether, this requires $\mathcal{O}(|\mathcal{K}| \cdot |\mathcal{M}| \cdot |\mathcal{N}| \cdot |\mathcal{P}| \cdot (|\mathcal{Q}| \cdot |\mathcal{R}|)^2)$ arithmetic operations. The following are typical index set sizes for the example applications of Section 6.

- $|\mathcal{R}|$ is the number of symbols for which the ISI shall be computed. For some example applications with optimally well time-frequency localized Gaussian

window g, Figure 12 below shows that $|\mathcal{R}|$ of size 4–5 is enough to cover a decay of the average ISI/ICI to 10^{-6} times the average of the diagonal entries. For other windows g, we expect a need for larger $|\mathcal{R}|$.

- $|\mathcal{Q}|$ is the number of carrier frequencies, which normally equals the number of samples per received symbol. In radio communications $|\mathcal{Q}|$ is typically in the range 128–1024. For the inherently more wideband underwater example in Section 6, much smaller $|\mathcal{Q}|$ is possible. With the window and lattice matching described in Section 5.3, $|\mathcal{Q}| = 47$ in our underwater example plots.

- $|\mathcal{K}|$ and $|\mathcal{M}|$ depend on the time-frequency localization of γ and g, respectively. For the Gaussian windows used below, $|\mathcal{K}| \cdot |\mathcal{M}| = 28 \cdot 19 = 532$ for the underwater channel and $|\mathcal{K}| \cdot |\mathcal{M}| = 19 \cdot 19 = 361$ for the other two.

- $|\mathcal{N}| \cdot |\mathcal{P}|$ is a constant that depends on $|\mathbf{\Omega}|$ and is proportional to the area $\langle \boldsymbol{\omega}, \boldsymbol{L} \rangle$ of the spreading function support. Below $|\mathcal{N}| \cdot |\mathcal{P}|$ equals $13 \cdot 27 = 351$, $13 \cdot 58 = 754$, and $59 \cdot 237 = 13983$ in the OFDM, satellite and underwater example, respectively.

Hence, if g and γ have roughly $M = |\mathcal{M}|$ nonzero Nyquist frequency samples, and if the received symbols have $Q = |\mathcal{Q}|$ nonzero Nyquist frequency samples and if $R = |\mathcal{R}|$, then our refined algorithm requires $R^2 \cdot \mathcal{O}(M^2 \cdot Q^2)$ arithmetic operations. This can be compared to the $R^2 \cdot \mathcal{O}(Q^5)$ operations of the more naive and straightforward matrix computation approach discussed in section 4, which is clearly slower when the number of carrier frequencies Q is larger than M.

Example 1. We show in Figure 7 that the Gaussian window approximation used in Section 6 has $M = 19$ Nyquist frequency samples. We can compare this with the B-spline windows $B_0 \stackrel{\text{def}}{=} I_{0,1}$ and $B_n \stackrel{\text{def}}{=} B_{n-1} * I_{0,1}$, which also were proposed in [MSG+05]. Since $\widehat{B_n}(\xi) = \operatorname{sinc}_1(\xi)^{n+1}$, its ϵ-essential support is contained in the interval $I_{0,\Omega}$ for which $1/(\pi\Omega/2)^{n+1} = \epsilon$, that is, $\Omega = 2\epsilon^{-1/(n+1)}/\pi$. Since the length of the support of B_n is $n+1$, M is now the smallest integer larger than $2\epsilon^{-1/(n+1)}(n+1)/\pi + 1$, which we plot for $\epsilon = 10^{-6}$ and some n in Figure 6. The smallest M is 25, which we get for B_{12}, B_{13} and B_{14}.

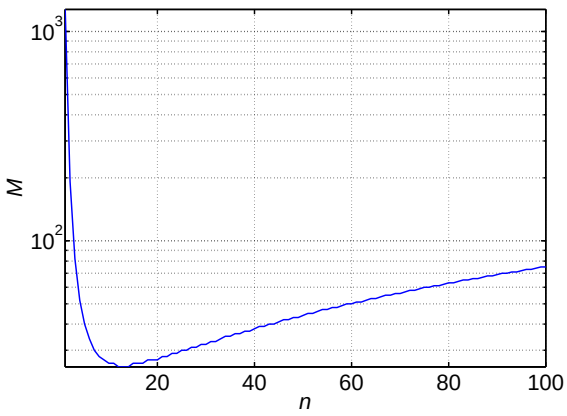

Figure 6: Number of nonzero Nyquist frequency samples for some B-splines B_n.

5.3 Parameters and window functions

In the operator discretizations (4.1), the shape of the Gabor window g can be optimized in different ways depending on the application. For wireless multicarrier systems, the pulse shaping of g is an active research topic in its own, which we do not pursue further here (see, for example, [MSG+05] for more details and references). We have already motivated in Section 4 that both bases should be Gabor bases with the same lattice parameters. For reasons described below, we choose to set the lattice "time" parameter to $\boldsymbol{aT_g}$ with $\boldsymbol{a} \in \mathbb{Z}_+$. Similarly, for some $\boldsymbol{b} \in \mathbb{R}_+^d$ we set the lattice frequency parameter to $\boldsymbol{b\Omega}$, so that the unit cell "area" $\boldsymbol{aT_g b\Omega} = \boldsymbol{ab}$ only depends on $\boldsymbol{a}$ and $\boldsymbol{b}$. In the examples of Section 6, we choose parameters so that $ab > 1$, which gives undersampling (see [Grö00]) and a Gabor system that is a Riesz basis for its span. In general, for finite index sets $\mathcal{Q} \times \mathcal{R}$, we will consider Gabor Riesz bases

$$g_{\boldsymbol{q},\boldsymbol{r}} = T_{\boldsymbol{raT_g}} M_{\boldsymbol{qb\Omega}} g \quad \text{and} \quad \gamma_{\boldsymbol{q},\boldsymbol{r}} = T_{\boldsymbol{raT_g}} M_{\boldsymbol{qb\Omega}} g, \qquad (\boldsymbol{q},\boldsymbol{r}) \in \mathcal{Q} \times \mathcal{R}. \tag{5.1a}$$

We are primarily interested in windows with very good joint time-frequency localization, which is of utmost importance for low ISI and ICI. Good frequency localization also allows for high transmission power and, therefore, large signal-to-noise ratio in the transmission band without exceeding power leakage bounds for other frequency bands. Such leakage is strictly regulated for radio communications, but not (yet) for underwater sonar communications, where, however, frequency bands already in use by, for example, the human ear or dolphins should be respected!

In the following, we shall use standard Gaussian windows

$$g(\boldsymbol{x}) = \mathrm{e}^{-\langle \boldsymbol{\alpha x}, \boldsymbol{x} \rangle}. \tag{5.1b}$$

Gaussian windows have optimal time-frequency localization [Grö00, Section 2.2], which results in very low ISI/ICI. This also has the advantage of making the effects of truncation to ϵ-essential support clearly visible in the plots of Section 6.

The window γ is set to $\gamma = Hg$ in the example applications of Section 6. Lower ISI/ICI can be obtained with other choices described in [MSG+05].

Other application-dependent parameters we choose in the following way:

1. *Index sets:* Choose the Gabor basis index set $\mathcal{R}$, the number of carrier frequencies $|\mathcal{Q}|$ and the desired minimum size of the index sets $\mathcal{N}$ and $\mathcal{P}$. Larger $|\mathcal{N}|$ and $|\mathcal{P}|$ can be used for obtaining better control of the smoothness and decay of $S_{\boldsymbol{\Omega_c''}}^{\boldsymbol{\Omega''}}$.

2. *Channel-dependent parameters:* For the channel at hand, choose the total allowed frequency band $[\boldsymbol{\Omega_0}, \boldsymbol{\Omega_1}]$, a "rectangle" $I_{\boldsymbol{\omega}_c,\boldsymbol{\omega}} \times I_{\boldsymbol{C},\boldsymbol{L}}$ containing the ϵ-essential support of S_H and the type of time-decay of S_H. (See Section 6 for examples.)

3. Choose the lattice constants $\boldsymbol{a}$ and $\boldsymbol{b}$, as well as the parameter $\boldsymbol{\alpha}$ in (5.1b), which uniquely determines the ϵ-essential support $\boldsymbol{\Omega} = \frac{1}{\boldsymbol{T_g}}$ of $\widehat{g}$. For non-Gaussian g, this step corresponds to the choice of a dilation parameter $\boldsymbol{\alpha}$ in an equation of the kind $g(\boldsymbol{x}) \stackrel{\text{def}}{=} g_0(\boldsymbol{\alpha x})$.

We have done the following choice, inspired by a similar design criterion in [KM98, Koz97, Mat00] For the smallest "rectangle" $I_{\boldsymbol{A}_c,\boldsymbol{A}} \times I_{\boldsymbol{B}_c,\boldsymbol{B}}$ that contains the ϵ-essential support of the short-time Fourier transform of g with window g (defined in (2.8)), choose $\boldsymbol{a}$, $\boldsymbol{b}$ and $\boldsymbol{\alpha}$ such that

$$\frac{\boldsymbol{\omega}}{\boldsymbol{L}} = \frac{\boldsymbol{B}}{\boldsymbol{A}} = \frac{\boldsymbol{b\Omega}}{\boldsymbol{aT_g}} \tag{5.2}$$

and such that $(g_{\boldsymbol{q},\boldsymbol{r}})$ is a Riesz basis for its span (obtained by setting $ab > 1$ in the results presented in Section 6). See [GP05] for details.

4. Choose $\mathcal{Q}$ so that the supports of all $\widehat{g_{\boldsymbol{q},\boldsymbol{r}}}$ are in the allowed frequency band $[\boldsymbol{\Omega_0}, \boldsymbol{\Omega_1}]$. Set $\boldsymbol{\Omega'_c}$ and $\boldsymbol{\Omega'}$ according to (4.13a). Set $\boldsymbol{\Omega''_c} = \boldsymbol{\Omega'_c}$ and choose $\boldsymbol{\Omega''}$ to be large enough to obtain the desired minimum size of $\mathcal{P}$ and also large enough to for the desired smooth truncation (4.13d) and (4.13e) ($\Omega'' \geq 1.5\Omega'$ in our implementation). Set $\boldsymbol{T_\gamma} = \frac{1}{\boldsymbol{\Omega}+\boldsymbol{\omega}}$ and $\boldsymbol{T''} = \frac{1}{\boldsymbol{\Omega''}}$.

5. Choose $\boldsymbol{L_0}$ and $\boldsymbol{C_0}$ so that (4.13b) holds and such that $\boldsymbol{L_0}$ is large enough to obtain the desired minimum size $|\mathcal{N}| = \frac{\boldsymbol{\omega}}{\boldsymbol{\omega_0}} = \boldsymbol{\omega L_0}$. Also set $\boldsymbol{\omega_0} = \frac{1}{\boldsymbol{L_0}}$.

6. Compute the Nyquist frequency samples of the restriction of g to its ϵ-essential support (as illustrated in Figure 7 (a)).

7. Compute the samples $S^{\boldsymbol{\Omega''}}_{\boldsymbol{\Omega''_c}}(\boldsymbol{n\omega_0}, \boldsymbol{pT''})$ that appear as coefficients in (4.14). There are basically two ways to obtain these coefficients:

   (a) Compute them from measurements or from a detailed model of a real channel.

   (b) Generate a random choice of the samples that satisfies the decay and support properties described in Section 3 and Section 6.

   For the results in Section 6 we have chosen approach (b).

6 Applications

We shall now describe parameter values and show sample plots for three channels with different spreading function support areas.

6.1 Mobile phone communications

For a mobile phone moving at 100 km/h, equations (3.2) imply that the maximum Doppler spread is $\frac{V_P}{V_w}\xi = 100/(299792.458 \cdot 3600)\xi \approx 10^{-7}\xi$. For the GSM mobile phone frequency bands ξ is ranging from 450.4–1990 MHz, so that frequency shifts caused by the Doppler effect is in the interval $[-184, 184]$ Hz. Typical time delays are of the order 10^{-6} s, so the spreading function support area is of size $4 \cdot 10^{-4}$. This support would exceed the critical value 1 (see page 11) if the highest channel frequencies in use exceed 5 THz. These are infrared light frequencies, for which the water in the Earth's atmosphere absorbs too strongly for us to expect these

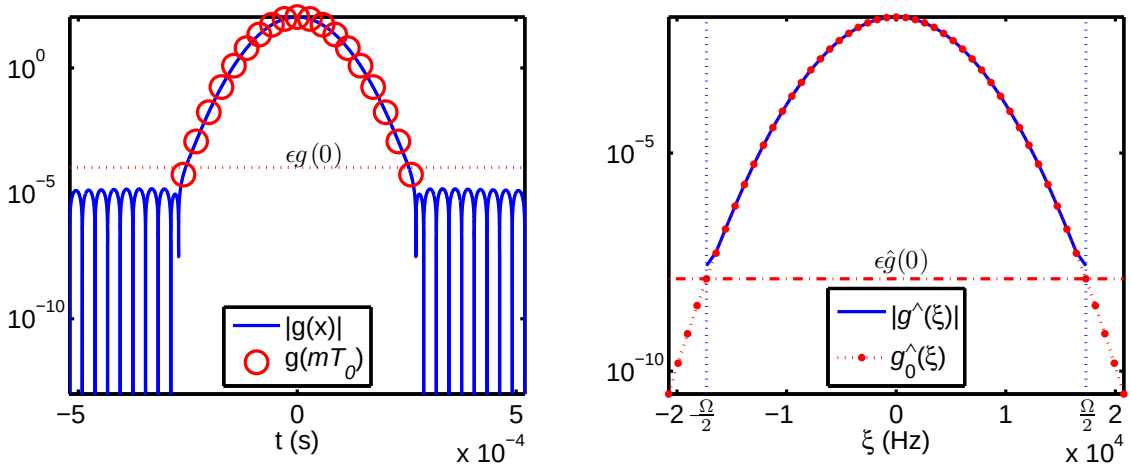

(a) (b)

Figure 7: We use the Gabor window/pulse shape g that we obtain from a Gaussian $g_0(x) = \mathrm{e}^{-\alpha x^2}$ by assuming $\widehat{g_0}$ to have bandwidth Ω given by its ϵ-essential support and truncating the reconstruction of g_0 from its Nyquist frequency samples to samples in the ϵ-essential support of g_0. We do this for $\epsilon = 10^{-6}$. Plots (a) and (b) show a comparison of the resulting g and $\widehat{g}$ with g_0 and $\widehat{g_0}$, respectively.

frequencies to be useful for wireless communications. Thus, with the terminology of Section 2.4, mobile phone channels are inherently underspread.

With other parameters chosen as described in Section 5.3, we obtain a Gaussian window g_0 with Fourier transform ϵ-essential support Ω. Hence we can approximate g_0 by reconstructing it from the Nyquist sampling theorem with sample interval $T_g = 1/\Omega$ and samples outside the ϵ-essential support of g_0 discarded. This construction gives a very small upper bound for both the supremum and the L^2-norm of the resulting truncation error when only a small number of nonzero samples are kept, as can be seen in the plots of g_0, g, $\widehat{g_0}$ and $\widehat{g}$ in Figure 7. In practice, ϵ should be chosen small enough for the resulting errors to be dominated by the overall noise level of the application at hand. For example, note in Figure 7 (a) how the truncation to a truly bandlimited g with a finite number of nonzero samples gives "Gaussian decay" down to amplitudes below ϵ and then a slowly decaying tail with negligible amplitude and L^2-norm. In this and the following examples, $\epsilon = 10^{-6}$.

We show some example plots in Figure 8 for a system with 128 carrier frequencies and 16 OFDM symbols. In (a) we show the ϵ-essential support of the short-time Fourier transform $\mathcal{V}_{g_{\boldsymbol{q},\boldsymbol{r}}} g_{\boldsymbol{q},\boldsymbol{r}}$ (defined in (2.8)) for some neighbouring basis functions $g_{\boldsymbol{q},\boldsymbol{r}}$, from which we se that we can expect nonzero ISI and ICI at least for basis functions at distance

$$\|(\boldsymbol{q},\boldsymbol{r}) - (\boldsymbol{q}',\boldsymbol{r}')\|_{l^2} \stackrel{\text{def}}{=} \sqrt{(\boldsymbol{q}-\boldsymbol{q}')^2 + (\boldsymbol{r}-\boldsymbol{r}')^2} \leq 4$$

in the Gabor lattice. In (b) we plot the "bandpass filtered spreading function" $S_{\boldsymbol{\Omega}_c''}^{\boldsymbol{\Omega}''}(\boldsymbol{\nu},\cdot)$ computed from its samples by using (4.13c) and (4.13f) in a way similar to the proof of Proposition 4 (see [GP05] for details). In this plot we have assumed an environment with a very large amount of small scatterers adding up to a white Gaussian noise distribution of the coefficient values (see Section 6.4 for examples with a "smother" spreading function with more correlated coefficients).

For plotting the coefficient operator matrix, we need to define a linear ordering of the index sets

$$\mathcal{Q}\times\mathcal{R} = \{q_0, q_0+1, q_0+2, \ldots, q_0+(|\mathcal{Q}|-1)\}\times\{r_0, r_0+1, r_0+2, \ldots, r_0+(|\mathcal{R}|-1)\}\,.$$

We have chosen to group together indices belonging to the same OFDM symbol by using the order

$$n_{q,r} \stackrel{\text{def}}{=} (r-r_0)\cdot|\mathcal{Q}| + q - q_0 + 1, \tag{6.1}$$

for which we have plotted the 10-logarithm of the matrix element amplitudes in Figure 8 (c). With this ordering, the matrix is divided into 16×16 submatrices, such that in each submatrix, r and r' are fixed. The submatrices for which $r = r'$ show the ICI of symbol number r. Submatrices for which $r \neq r'$ show the ISI between OFDM symbols number r and r'.

Due to the matching of the Gabor lattice and the shape of the frequency localization of g to the shape of the spreading function support, which we explained in Section 5.3, the size of $|\langle H g_{\boldsymbol{q},\boldsymbol{r}}, \gamma_{\boldsymbol{q}',\boldsymbol{r}'}\rangle|$ should mainly depend on the distance $\|(\boldsymbol{q},\boldsymbol{r}) - (\boldsymbol{q}',\boldsymbol{r}')\|_{l^2}$ between the time-frequency support centerpoints in the Gabor lattice. For making this off-diagonal decay more visible, we have grouped together

matrix elements for which this distance is the same and plotted the average amplitude in Figure 8 (d). Note the clearly visible effect that occurs at distances more than four, which is caused by the truncations of windows and spreading functions to their ϵ-essential support.

6.2 Satellite communications

The speed of a communications satellite in geostationary orbit is about 3 km per second. Thus the maximum Doppler shift is $\frac{V_{\mathrm{P}}}{V_{\mathrm{w}}}\xi = (3/299792.458)\xi \approx 10^{-5}\xi$. With typical transmission frequencies 1-30 GHz [MB02], we can expect Doppler shifts up to some 10^4 Hz. Here, we will use an example from [MB02, p. 47] with transmission frequency 6 GHz and Doppler shift 18 kHz. Again, we assume the maximum time-spread to be some 10^{-6} s. Then the spreading function support area is less than

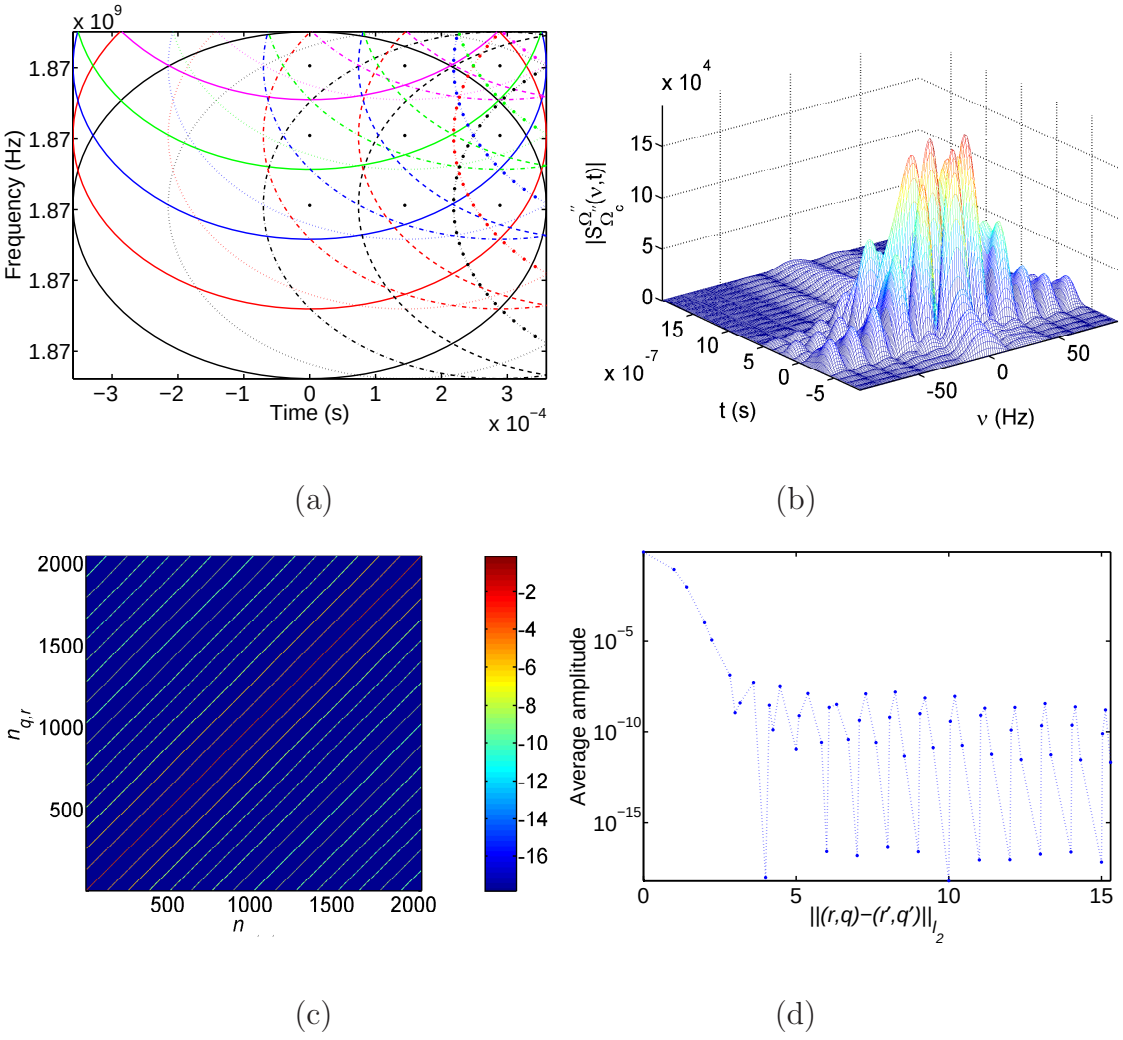

Figure 8: OFDM channel example. (a) ϵ-essential support of the short-time Fourier transform $\mathcal{V}_{g_{\boldsymbol{q},\boldsymbol{r}}} g_{\boldsymbol{q},\boldsymbol{r}}$ for some neighbouring basis functions $g_{\boldsymbol{q},\boldsymbol{r}}$. (b) The spreading function. (c) The 10-logarithm of $|\langle H g_{\boldsymbol{q},\boldsymbol{r}}, \gamma_{\boldsymbol{q}',\boldsymbol{r}'}\rangle|$ with index ordering $n_{q,r}$ defined in (6.1). (d) Off-diagonal decay.

0.036, so this is an underspread channel as well.

We show the same plots as for the OFDM example in Figure 9. Note that as a result of the window and lattice constant matching, the plots (a) in Figure 8 an 9 are largely the same up to scaling.

6.3 Underwater sonar communications

For a vehicle travelling at 30 knot in sea water and using sonar communications, we have $\frac{V_{\mathrm{P}}}{V_{\mathrm{w}}}\xi \approx \frac{30 \cdot 0.51444}{1531}\xi \approx 10^{-2}\xi$. We will use parameters typical for some medium range systems described in [Sto99] with maximum time spread around 0.01 s and a typical frequency band 20-35 kHz, so that the maximum Doppler shift is about 350 Hz. (More examples can be found, for example, in [LO97, Mid87, Sto96, ZK00, ZT02].) These settings give spreading function support area 7 and an overspread

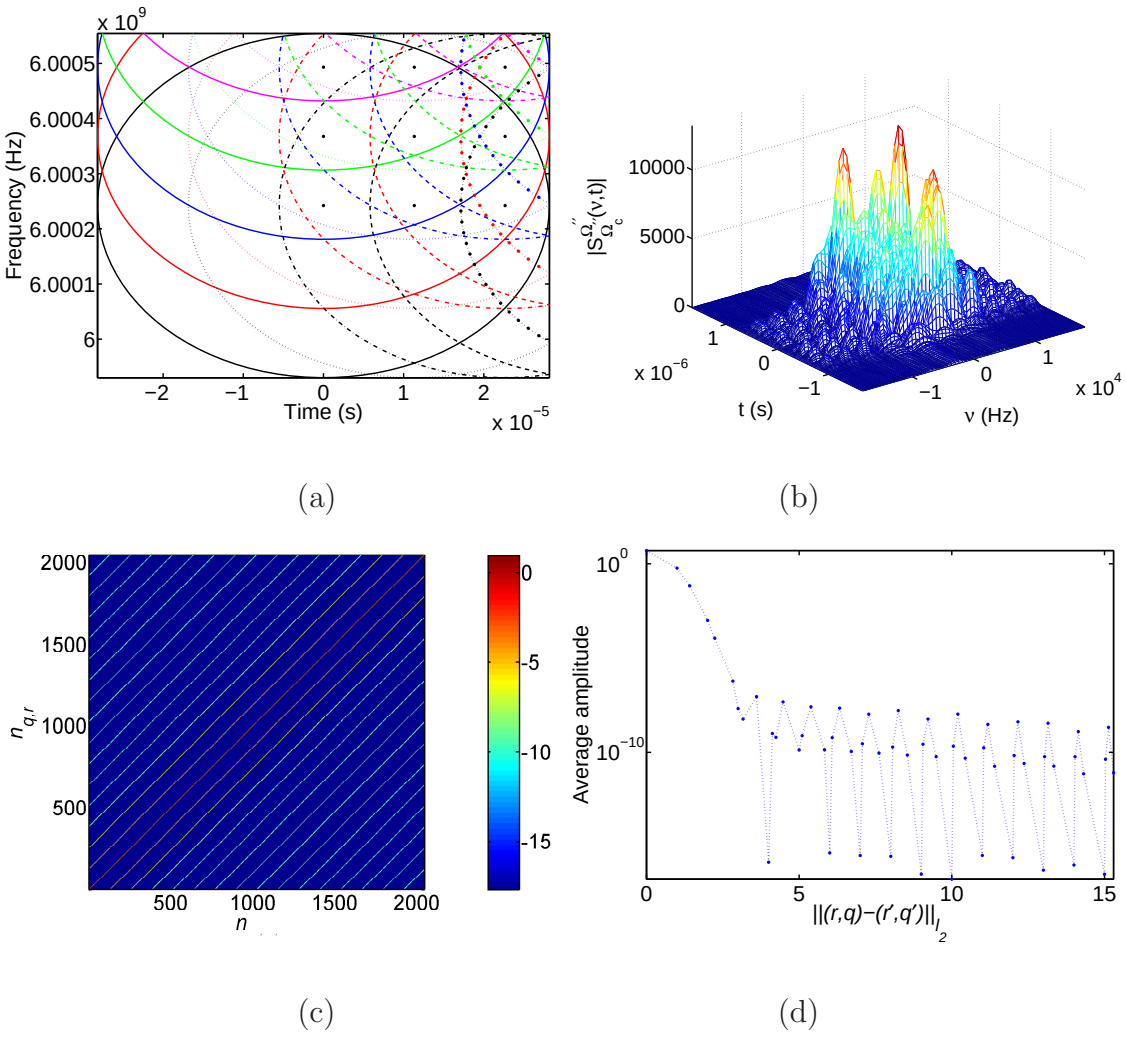

Figure 9: Satellite channel example. (a) ϵ-essential support of the short-time Fourier transform $\mathcal{V}_{g_{q,r}} g_{\boldsymbol{q},\boldsymbol{r}}$ for some neighbouring basis functions $g_{\boldsymbol{q},\boldsymbol{r}}$. (b) The spreading function. (c) The 10-logarithm of $|\langle H g_{\boldsymbol{q},\boldsymbol{r}}, \gamma_{\boldsymbol{q}',\boldsymbol{r}'}\rangle|$ with index ordering $n_{q,r}$ defined in (6.1). (d) Off-diagonal decay.

channel, which is typical for underwater sonar communications channels in general.

We show the same plots as for the previous two examples in Figure 10.

6.4 Further spreading function examples

In the above examples we used independent Gaussian distributions to obtain the spreading function coefficients. For a "nicer" environment, one can expect more correlation between the samples. We show examples of such spreading functions in Figure 11. In Figure 12 we compare these two different spreading functions with all other channel parameters being identical. The plots show that these two different correlations of the spreading function samples do not affect the speed of the off-diagonal decay significantly.

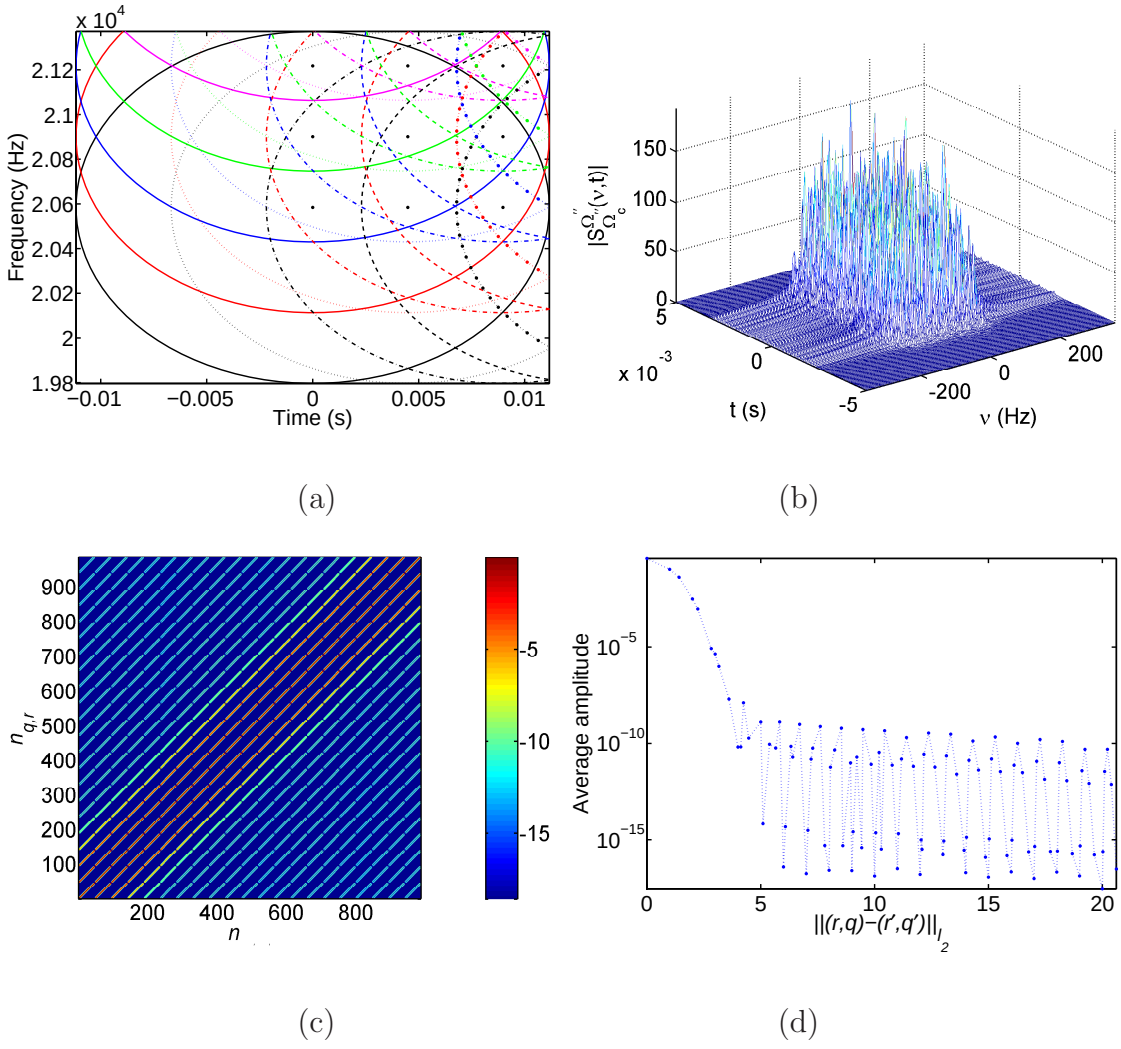

Figure 10: Underwater channel example. (a) ϵ-essential support of the short-time Fourier transform $\mathcal{V}_{g_{q,r}} g_{\boldsymbol{q},\boldsymbol{r}}$ for some neighbouring basis functions $g_{\boldsymbol{q},\boldsymbol{r}}$. (b) The spreading function. (c) The 10-logarithm of $|\langle H g_{\boldsymbol{q},\boldsymbol{r}}, \gamma_{\boldsymbol{q}',\boldsymbol{r}'}\rangle|$ with index ordering $n_{q,r}$ defined in (6.1). (d) Off-diagonal decay.

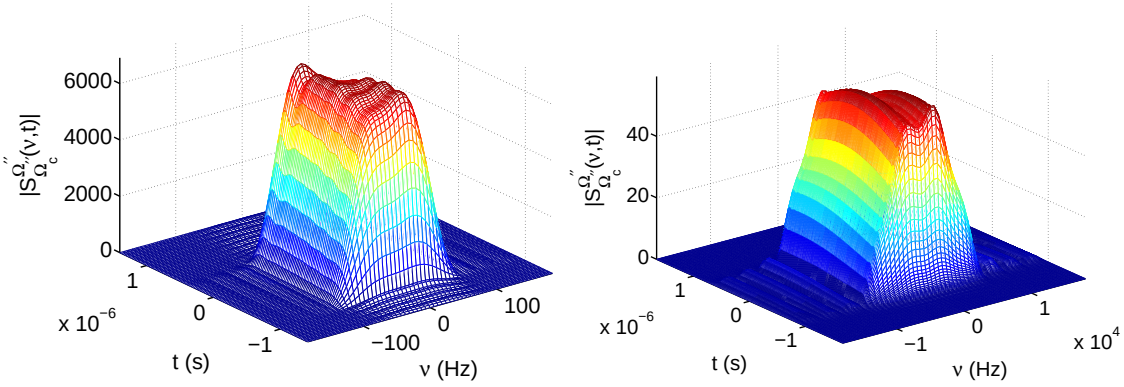

(a) (b)

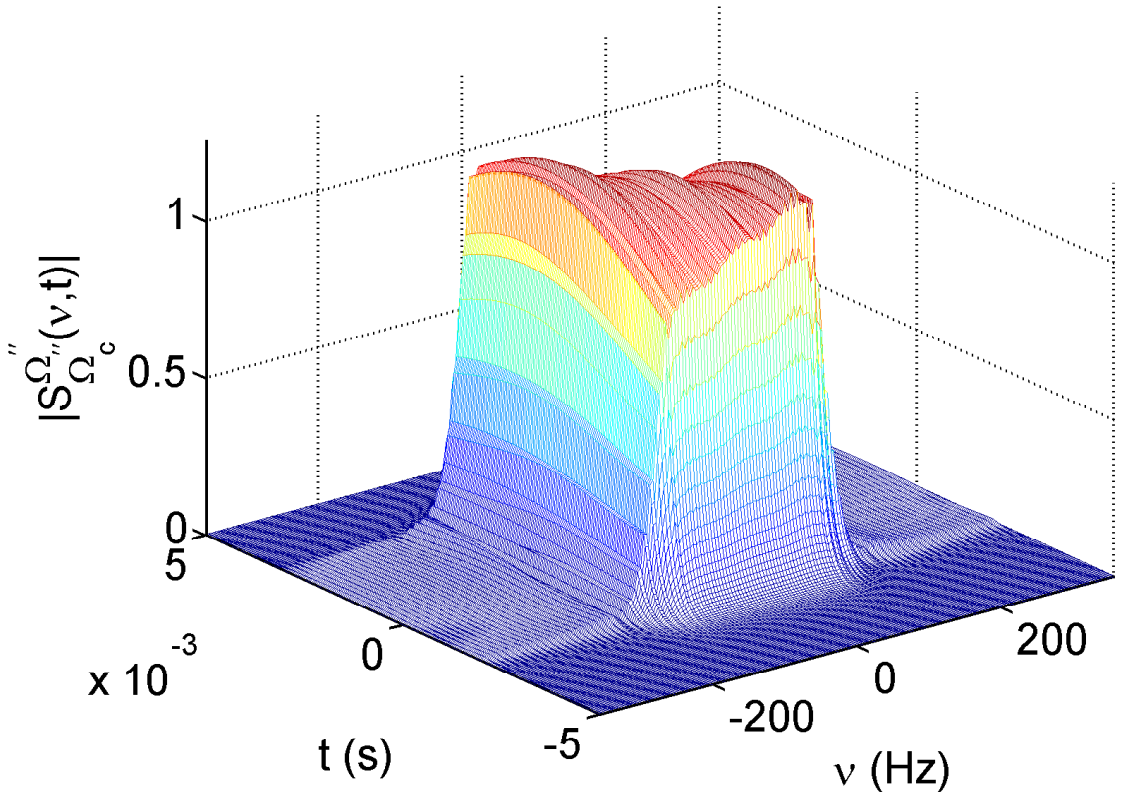

(c)

Figure 11: Spreading functions with more correlated coefficients $S^{\Omega''}_{\Omega''_c}(\boldsymbol{n\omega_0}, \boldsymbol{pT''})$. (a)–(c) shows the spreading functions for the OFDM, satellite and underwater example, respectively. Figure 12 shows a comparison of the resulting off-diagonal decays with those in figures 8–10.

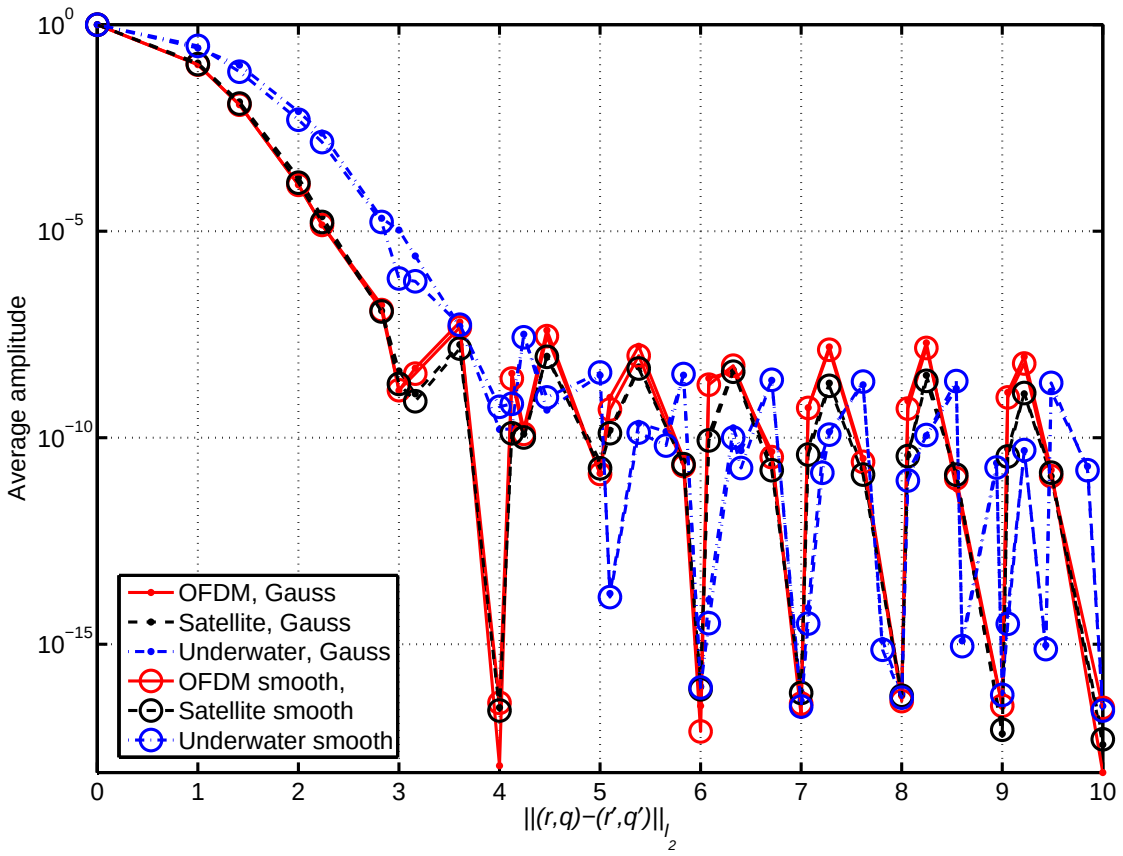

Figure 12: Off-diagonal decays with spreading function coefficients normalized so that the average of $\|Hg_{\boldsymbol{q},\boldsymbol{r}}\|_2$ equals one.

7 Conclusions

Using a refinement of the standard multipath propagation model for the short time behaviour of narrowband wireless channels, we have derived a spreading function integral representation of such channels with a C^∞ spreading function with subexponential decay.

This, together with a channel discretization using well time-frequency localized Gabor bases, allowed us to derive formulas and an algorithms for the efficient computation of certain matrix representations of communication channels. The elements of this matrix describe the intersymbol and intercarrier interference for the transmitted signal. We derived the algorithm, as well as some refinements of it, under a minimum of assumptions or simplifications beyond the channel and signal properties that are known from our channel and signal model.

Next, we discussed parameter choices in general and for three different channels. For these channels we used a MATLAB implementation of our algorithm to compute example plots showing the time-frequency localization of the Gabor basis functions, the spreading functions, the coefficient operator matrix, and its off-diagonal decay.

Our implementation is fast enough for at least 2048×2048 matrices and considerably faster than a simpler and more straightforward approach to computing the matrix elements.

Due to bandwidth and delay restrictions, multicarrier communications must use bandlimited basis functions defined by a finite number of nonzero Nyquist frequency samples. Our plots show clearly how such restrictions affect the off-diagonal decay of the coefficient operator matrix. Thus the algorithm and software can be useful for the numerical comparisons of the off-diagonal decay for different pulse shapes and parameter settings.

Moreover, although we primarily consider communications applications in this paper, we derived our algorithm in a more general multivariate setting, as an analysis tool for certain classes of Hilbert Schmidt operators with potential other theoretical and practical applications.

Acknowledgements: We want to thank Dr. Werner Kozek at Siemens AG in Vienna, Austria, and Professor Harald Haas at International University Bremen, Germany, for insightful discussions about the physical properties of wireless channels. We are also thankful to Professor Karlheinz Gröchenig at the Numerical Harmonic Analysis Group in Vienna, Austria, for providing the references on which Section 2.1 is based.

References

[Bel63] Philip A. Bello. Characterization of randomly time-variant linear channels. *IEEE T. Commun. Syst.*, 11:360–393, December 1963. WWW: `http://ieeexplore.ieee.org/xpl/abs_free.jsp?arNumber=1088793`.

[Bel64] P. Bello. Time-frequency duality. *IEEE Trans. Inform. Theory*, 10(1):18–33, 1964. WWW: `http://ieeexplore.ieee.org/xpl/abs_free.jsp?arNumber=1053640`.

[Beu38] A. Beurling. Sur les intégrales de Fourier absolument convergentes et leur application à une transformation fonctionnelle. In *Neuvième congrès des mathématiciens scandinaves*, Helsingfors, 1938. Reprinted as [Beu89, p. 39–60].

[Beu89] Arne Beurling. *The Collected Works of Arne Beurling. Volume 2, Harmonic Analysis*, volume 2. Birkhäuser, Boston ; Basel, 1989.

[BLM04] Imad Barhumi, Geert Leus, and Marc Moonen. Time-domain and frequency-domain per-tone equalization for OFDM over doubly selective channels. *Signal Process.*, 84(11):2055–2066, November 2004. WWW: `http://www.sciencedirect.com/science/journal/01651684`.

[BLM05] Imad Barhumi, Geert Leus, and Marc Moonen. Time-varying FIR equalization for doubly selective channels. *IEEE T. Wirel. Commun.*, 4(1):202–214, January 2005. WWW: `http://ieeexplore.ieee.org/xpl/abs_free.jsp?arnumber=1381438`.

[BS01] Scott Beaver and Thomas Strohmer. Optimal OFDM pulse and lattice design for doubly dispersive channels. In *Conference Record of the Thirty-Fifth Asilomar Conference on Signals, Systems and Computers*, pages 1763–1767, Pacific Grove, CA, USA, 2001. WWW: `http://www.math.ucdavis.edu/~strohmer`.

[CB00] Podvoiski Carstens-Behrens. Estimation of combustion chamber resonances for improved knock detection in spark ignition engines. In *Proc. 18. CAD-FEM Users' Meeting, Internationale FEM-Technologietage*, Friedrichshafen, September 2000. WWW: `http://www.sth.rub.de/de/index.html`.

[CBB01] Sönke Carstens-Behrens and Johann F. Böhme. Fast knock detection using pattern signals. In *Proc. IEEE ICASSP 2001*, (SAE technical paper: 2002-01-0237), pages 3145–3148, Salt Lake City, UT, May 2001. WWW: `http://www.sth.rub.de/de/index.html`.

[CBUB+02] Sönke Carstens-Behrens, Mark Urlaub, Johann F. Böhme, Jürgen Förster, and Franz Raichle. FEM approximation of internal combustion chambers for knock investigations. In *SAE 2002 World Congress & Exhibition*, (SAE technical paper: 2002-01-0237), Detroit, MI, USA, March 2002. WWW: `http://www.sth.rub.de/de/index.html`.

[CBWB99] Sönke Carstens-Behrens, Michel Wagner, and Johann F. Böhme. Improved knock detection by time variant filtered structure-borne sound. In *Proc. IEEE ICASSP '99*, volume 4, pages 2255–2258, Phoenix, March 1999. WWW: `http://www.sth.rub.de/de/index.html`.

[Chr02] Ole Christensen. *An Introduction to Frames and Riesz Bases*. Birkhäuser, 2002.

[Con00] John B. Conway. *A course in operator theory*. 2000.

[DH98] Jacek Dziubański and Eugenio Hernández. Band-limited wavelets with subexponential decay. *Canad. Math. Bull.*, 41(4):398–403, 1998. WWW: `http://www.journals.cms.math.ca/CMB/v41n4/index.en.html`.

[Dom56] Y. Domar. Harmonic analysis based on certain commutative Banach algebras. *Acta Math.*, 96:1–66, 1956.

[EG04] Stefan Ericsson and Niklas Grip. Efficient wavelet pre-filters with optimal time-shifts. *IEEE Trans. Signal Process.*, 53(7):2451–2461, July 2004. WWW: `http://www.sm.luth.se/~grip/Research/publications.php`.

[EG05] Stefan Ericsson and Niklas Grip. An analysis method for sampling in shift-invariant spaces. *Int. J. Wavelets Multiresolut. Inf. Process.*, 3(3):301–319, September 2005. WWW: `http://www.sm.luth.se/~grip/Research/publications.php`.

[FK98] Hans G. Feichtinger and Werner Kozek. Quantization of TF lattice–invariant operators on elementary LCA groups. In Hans G. Feichtinger and Thomas Strohmer, editors, *Gabor Analysis and Algorithms*, chapter 7, pages 233–266. Birkhäuser, Boston, MA, USA, 1998.

[Fol95] Gerald B Folland. *A Course in Abstract Harmonic Analysis*. Studies in advanced mathematics. CRC Press, Boca Raton, FL, 1995.

[Fol99] Gerald B. Folland. *Real analysis. Modern techniques and their applications*. Pure and Applied Mathematics. A Wiley-Interscience Series of Texts, Monographs, and Tracts., NY, second edition, 1999.

[FZ98] Hans G. Feichtinger and Georg Zimmermann. A Banach space of test functions for Gabor analysis. In Hans G. Feichtinger and Thomas Strohmer, editors, *Gabor Analysis and Algorithms*, chapter 3, pages 123–170. Birkhäuser, Boston, MA, USA, 1998.

[GHS+01] Calle Gustavsson, Christian Henriksson, Mårten Sander, Peter Sidén, Roland Standert, and Andreas Vedin. Full duplex OFDM modem over a frequency selective channel. Project course report, Department of Signals, Sensors and Systems, KTH, Stockholm, Sweden, May 2001. WWW: `http://www.s3.kth.se/signal/edu/projekt/students/01/lightbrown/www/fina`

[GP05] Niklas Grip and Götz Pfander. Time varying narrowband communications cannels: Analysis and implementation. Research report, School of Engineering and Science, International University Bremen, 2005.

[Gri02] Niklas Grip. *Wavelet and Gabor Frames and Bases: Approximation, Sampling and Applications.* Doctoral thesis 2002:49, Luleå University of Technology, SE-971 87 Luleå, 2002. WWW: http://www.sm.luth.se/∼grip/Research/publications.php.

[Grö00] Karlheinz Gröchenig. *Foundations of Time-Frequency Analysis.* Birkhäuser, 2000.

[Hör03] Lars Hörmander. *The Analysis of Linear Partial Differential Operators I; Distribution Theory and Fourier Analysis.* Classics in mathematics. Springer, second edition, 2003.

[Jan98] A. J. E. M. Janssen. The duality condition for Weyl-Heisenberg frames. In Hans G. Feichtinger and Thomas Strohmer, editors, *Gabor Analysis and Algorithms*, chapter 1, pages 33–84. Birkhäuser, Boston, MA, USA, 1998.

[Kat04] Yitzhak Katznelson. *An Introduction to Harmonic Analysis.* Cambridge University Press, third corrected edition, 2004.

[KM98] Werner Kozek and Andreas F. Molisch. Nonorthogonal pulseshapes for multicarrier communications in doubly dispersive channels. *IEEE J. Sel. Area. Comm.*, 16(8):1579–1589, October 1998. WWW: http://ieeexplore.ieee.org/iel4/49/15739/00730463.pdf.

[Koz97] Werner Kozek. *Matched Weyl-Heisenberg Expansions of Nonstationary Environments.* Ph.D. thesis, Technical University of Vienna, March 1997. WWW: http://www.mat.univie.ac.at/ nuhag/papers/1997/koz0897.html.

[KP06] W. Kozek and G.E. Pfander. Identification of operators with bandlimited symbols. *SIAM J. Math. Anal.*, 37(3):867–888, 2006 2006.

[KPZ02] Werner Kozek, Götz Pfander, and Georg Zimmermann. Perturbation stability of coherent Riesz systems under convolution operators. *Appl. Comput. Harmon. Anal.*, 12(3):286–308, May 2002. WWW: http://www.math.iu-bremen.de/pfander/publications.php.

[LM04] Geert Leus and Marc Moonen. Equalization techniques for fading channels. In Mohamed Ibnkahla, editor, *Handbook on Signal Processing for Communications*, chapter 16, pages 16.1–16.30. CRC Press, 2004.

[LO97] W. K. Lam and R. F. Ormondroyd. A coherent COFDM modulation system for a time-varying frequency-selective underwater acoustic channel. In *Seventh International Conference on Electronic Engineering in Oceanography : technology transfer from research to industry*, pages 198–203, Southampton, UK, June 1997. IEEE. WWW: http://ieeexplore.ieee.org/xpl/abs_free.jsp?arNumber=612669.

[LPW05] James Lawrence, Götz Pfander, and David Walnut. Linear independence of Gabor systems in finite dimensional vector spaces. *J. Fourier Anal. Appl.*, 11(6):715–726, 2005. To appear. WWW: http://www.math.iu-bremen.de/pfander/publications.php.

[LZG03] Geert Leus, Shengli Zhou, and Georgios B. Giannakis. Orthogonal multiple access over time- and frequency-selective channels. *IEEE Trans. Inform. Theory*, 49(8):1942–1950, August 2003. WWW: http://ieeexplore.ieee.org/xpl/abs_free.jsp?arNumber=1214073.

[Mat00] Gerald Matz. *A Time-Frequency Calculus for Time-Varying Systems and Nonstationary Processes with Applications.* Ph.d. thesis, Vienna University of Technology, November 2000. WWW: http://www.lss.supelec.fr/perso/matz_gerald.OLD/GM_other.html.

[MB02] Gérard Maral and Michel Bousquet. *Satellite Communications Systems: Systems, Techniques and Technology.* John Wiley & Sons, fourth edition, 2002.

[MG02] Xiaoli Ma and Georgios B. Giannakis. Maximum-diversity transmissions over time-selective wireless channels. In *Wireless Communications and Networking Conference, 2002. (WCNC2002)*, volume 1, pages 497–501, March 2002. WWW: http://ieeexplore.ieee.org/xpl/abs_free.jsp?arNumber=993547.

[MG03a] Xiaoli Ma and Georgios B. Giannakis. Full-diversity full-rate complex-field space-time coding. *IEEE Trans. Signal Process.*, 51(11):2917–2930, November 2003. WWW: http://ieeexplore.ieee.org/xpl/abs_free.jsp?arNumber=1237423.

[MG03b] Xiaoli Ma and Georgios B. Giannakis. Maximum-diversity transmissions over doubly selective wireless channels. *IEEE Trans. Inform. Theory*, 49(7):1832–1840, July 2003. WWW: http://ieeexplore.ieee.org/xpl/abs_free.jsp?arNumber=1207384.

[MH99] Gerald Matz and Franz Hlawatsch. Time-frequency subspace detectors and application to knock detection. *AEÜ Int. J. Electron. Commun.*, 53(6):379–385, 1999. WWW: http://www.lss.supelec.fr/perso/matz_gerald/GM_jrnl.html.

[Mid87] D. Middleton. Channel modeling and threshold signal processing in underwater acoustics: An analytical overview. *IEEE J. Oceanic Eng.*, 12(1):4–28, January 1987. WWW: http://ieeexplore.ieee.org/xpl/abs_free.jsp?arNumber=1145225.

[MLG05] Xiaoli Ma, Geert Leus, and Georgios B. Giannakis. Space-time-Doppler block coding for correlated time-selective fading channels. *IEEE Trans. Signal Process.*, 53(6):2167–2181, June 2005. WWW: http://ieeexplore.ieee.org/xpl/abs_free.jsp?arNumber=1433146.

[MMH+02] Gerald Matz, Andreas F. Molisch, Franz Hlawatsch, Martin Steinbauer, and Ingo Gaspard. On the systematic measurement errors of correlative mobile radio channel sounders. *IEEE T. Commun.*, 50(5):808–821, May 2002. WWW: http://www.lss.supelec.fr/perso/matz_gerald/GM_jrnl.html.

[MSG+05] G. Matz, D. Schafhuber, K. Gröchenig, M. Hartmann, and F. Hlawatsch. Analysis, optimization, and implementation of low-interference wireless multicarrier systems. *preprint*, 2005.

[PW05] G. E. Pfander and D. Walnut. Measurement of time-variant linear channels. *preprint*, 2005.

[Rap02] Theodore S. Rappaport. *Wireless communications: principles and practice*. Prentice Hall PTR, second edition, 2002.

[Reu74] D. O. Reudnik. Large-scale variations of the average signal. In William C. Jakes, editor, *Microwave Mobile Communications*, chapter 2, pages 79–131. John Wiley & Sons, NY, 1974. IEEE 1994 reprint with corrections.

[Ric03] Scott Rickard. *Time-frequency and time-scale representations of doubly spread channels*. Ph.D. dissertation, Princeton University, November 2003.

[RS80] Michael Reed and Barry Simon. *Methods of modern mathematical physics; I: Functional analysis*. Academic Press, NY, revised and enlarged edition edition, 1980.

[RS00] Hans Reiter and Jan D. Stegeman. *Classical Harmonic Analysis and Locally Compact Groups*. Number 22 in London Mathematical Society monographs; New Series. Oxford University Press, second edition, 2000.

[Rud87] Walter Rudin. *Real and Complex Analysis*. McGraw-Hill, third edition, 1987.

[SA99] Akbar M. Sayeed and Behnaam Aazhang. Joint multipath-Doppler diversity in mobile wireless communications. *IEEE T. Commun.*, 47(1):123–132, January 1999. WWW: http://ieeexplore.ieee.org/xpl/abs_free.jsp?arNumber=00747819.

[Sto96] Milica Stojanovic. Recent advances in high-speed underwater acoustic communications. *IEEE J. Oceanic Eng.*, 21(2):125–136, April 1996. WWW: http://intl.ieeexplore.ieee.org/xpl/tocresult.jsp?isNumber=27330&puNumb

[Sto99] Milica Stojanovic. *Underwater Acoustic Communications*, volume 22, pages 688–698. John Wiley & Sons, 1999. WWW: http://www.mit.edu/people/millitsa/publications.html.

[Str05] Thomas Strohmer. Pseudodifferential operators and Banach algebras in mobile communications. *Submitted to Appl.Comp.Harm.Anal.*, 2005. WWW: `http://www.math.ucdavis.edu/~strohmer`.

[TL04] Jitendra K. Tugnait and Weilin Luo. Blind identification of time-varying channels using multistep linear predictors. *IEEE Trans. Signal Process.*, 52(6):1739–1749, June 2004. WWW: `http://ieeexplore.ieee.org/xpl/abs_free.jsp?arNumber=01299106`.

[Zad50] Lofti A. Zadeh. Frequency analysis of variable networks. *Proc. IRE*, 38(3):291–299, March 1950.

[ZK00] Y.V. Zakharov and V.P. Kodanev. Multipath-Doppler diversity of OFDM signals in an underwater acoustic channel. In *Proceedings of ICASSP'2000*, volume 5, pages 2941–2944. IEEE, June 2000. WWW: `http://ieeexplore.ieee.org/xpl/abs_free.jsp?arNumber=861150`.

[ZT02] M. Zatman and B. Tracey. Underwater acoustic mimo channel capacity. In *Conference Record of the Thirty-Sixth Asilomar Conference on Signals, Systems and Computers*, volume 2, pages 1364–1368. IEEE, November 2002. WWW: `http://intl.ieeexplore.ieee.org/xpl/abs_free.jsp?arNumber=1197002`.